

1 **KGML-ag: A Modeling Framework of Knowledge-Guided Machine
2 Learning to Simulate Agroecosystems: A Case Study of Estimating
3 N₂O Emission using Data from Mesocosm Experiments**

4 Licheng Liu¹, Shaoming Xu², Jinyun Tang³⁴, Kaiyu Guan^{45,56,67}, Timothy J. Griffis⁷⁸, Matthew D.
5 Erickson⁷⁸, Alexander L. Frie⁷⁸, Xiaowei Jia⁸⁹, Taegon Kim^{1,9}, Lee T. Miller⁷⁸, Bin Peng^{45,56,67}, Shaowei
6 Wu¹⁰, Yufeng Yang¹, Wang Zhou^{45,56}, Vipin Kumar², Zhenong Jin^{1,11,3*}

7 ¹Department of Bioproducts and Biosystems Engineering, University of Minnesota, Saint Paul, MN, 55108, USA

8 ²Department of Computer Science and Engineering, University of Minnesota, Minneapolis, MN, 55455, USA

9 ³Institute on the Environment, University of Minnesota, Saint Paul, MN, 55108, USA

10 ⁴Climate and Ecosystem Sciences Division, Lawrence Berkeley National Laboratory, Berkeley, CA 94720, USA

11 ⁵Agroecosystem Sustainability Center, Institute for Sustainability, Energy, and Environment, University of Illinois at Urbana-Champaign, Urbana, IL 61801, USA

12 ⁶Department of Natural Resources and Environmental Sciences, University of Illinois at Urbana-Champaign, Urbana, IL 61801, USA

13 ⁷National Center for Supercomputing Applications, University of Illinois at Urbana-Champaign, Urbana, IL 61801, USA

14 ⁸Department of Soil, Water, and Climate, University of Minnesota, Saint Paul, MN 55108, USA

15 ⁹Department of Computer Science, University of Pittsburgh, Pittsburgh, PA, 15260, USA

16 ¹⁰Department of Smart Farm, Jeonbuk National University, Jeonju, Jeollabuk-do, 54896, Republic of Korea

17 ¹¹School of Physics and Astronomy, University of Minnesota, Minneapolis, MN, 55455, USA

18 ¹¹Institute on the Environment, University of Minnesota, Saint Paul, MN, 55108, USA

22 Correspondence to: Zhenong Jin (jinzn@umn.edu)

23 **Abstract.**

24 Agricultural nitrous oxide (N₂O) emission accounts for a non-trivial fraction of global greenhouse gases (GHGs) budget. To
25 date, estimating N₂O fluxes from cropland remains a challenging task because the related microbial processes (e.g., nitrification
26 and denitrification) are controlled by complex interactions among climate, soil, plant and human activities. Existing approaches
27 such as process-based (PB) models have well-known limitations due to insufficient representations of the processes or
28 uncertaintiesconstraints of model parameters, and to leverage recent advances in machine learning (ML) ^a new method is
29 needed to unlock the “black box” to overcome its limitations such asdue to low interpretability, out-of-sample failure and
30 massive data demand. In this study, we developed a firstoftheits kind knowledge-guided machine learning model for
31 agroecosystems (KGML-ag), by incorporating biogeophysical/chemical domain knowledge from an advanced PB model,
32 *ecosys*, and tested it by comparing simulating daily N₂O fluxes with real observed data from mesocosm experiments. The
33 Gated Recurrent Unit (GRU) was used as the basis to build the model structure. To optimize the model performance, we have
34 investigated a range of ideas, including: 1) Using initial values of intermediate variables (IMVs) instead of time series as model
35 input to reduce data demand; 2) Building hierarchical structures to explicitly estimate IMVs for further N₂O prediction; 3)
36 Using multitask learning to balance the simultaneous training on multiple variables; and 4) Pretraining with millions of
37 synthetic data generated from *ecosys* and fine tuning with mesocosm observations. Six other pure ML models were developed

Formatted: Border: Top: (No border), Bottom: (No border),
Left: (No border), Right: (No border), Between : (No border)

Formatted: Font color: Auto

Formatted: Font color: Auto

Formatted: Border: Top: (No border), Bottom: (No border),
Left: (No border), Right: (No border), Between : (No border)

38 using the same mesocosm data to serve as the benchmark for the KGML-ag model. Results show that KGML-ag did an
39 excellent job in reproducing the mesocosm N_2O fluxes (overall $r^2 = 0.81$, and $\text{RMSE} = 3.6 \text{ mg N m}^{-2} \text{ day}^{-1}$ from cross-
40 validation). Importantly KGML-ag always outperforms the PB model and ML models in predicting N_2O fluxes, especially for
41 complex temporal dynamics and emission peaks. Besides, KGML-ag goes beyond the pure ML models by providing more
42 interpretable predictions as well as pinpointing desired new knowledge and data to further empower the current KGML-ag.
43 We believe the KGML-ag development in this study will stimulate a new body of research on interpretable ML for
44 biogeochemistry and other related geoscience processes.

45 1 Introduction

46 Nitrous oxide (N_2O), with its global warming potential 273 ± 118 times greater than that of carbon dioxide (CO_2) for a 100-
47 year time horizon, is one of the [major important](#) greenhouse gases (IPCC6; Forster et al., 2021). The increasing rate of
48 atmospheric N_2O concentration during the period 2010-2015 is 44% higher than during 2000-2005, mainly driven by increased
49 anthropogenic sources that have increased total global N_2O emissions to $\sim 17 \text{ Tg N yr}^{-1}$ (Syakila and Kroeze, 2011; Thompson
50 et al., 2019). It is estimated that approximately 60% of the contemporary N_2O emission increases are from agriculture
51 management at global scale (Pachauri et al., 2014; Robertson et al., 2014; Tian et al., 2020), but the estimation uncertainty can
52 exceed 300% (Barton et al., 2015; Solazzo et al., 2021). Quantifying N_2O emissions from agricultural soils is extremely
53 challenging, partly because the related microbial processes, mainly about incomplete denitrification and nitrification, are
54 controlled by many environment and management factors such as temperature/water conditions, soil/crop properties, and N
55 fertilization rate, all of which together have collectively led to large temporal and spatial variabilities of N_2O emissions
56 (Butterbach-Bahl et al., 2013; Grant et al., 2016).

57 Process-based (PB) models are often used for simulating N_2O fluxes from [the agroecosystems](#), but they have some inherent
58 limitations, including incomplete knowledge of the processes, low accuracy due to the under-constrained parameters,
59 expensive computing cost, and rigid structure for further improvements, that we could not resolve by using PB model itself.
60 For example, an advanced agroecosystem model, *ecosys* (Grant et al., 2003, 2006, 2016), simulates N_2O production rates
61 through nitrification and denitrification processes when oxygen (O_2) is limited, with equations considering the influence from
62 related substrate concentrations (e.g., NO_2^- , N_2O , and CO_2), nitrifier and denitrifier populations, and soil thermal, hydrological
63 physical and chemical conditions. The produced N_2O accumulates, transfers in gaseous phase, aqueous phase, over different
64 soil layers, and eventually exchanges with atmosphere at the soil surface. Other PB models, including DNDC (Zhang et al.,
65 2002; Zhang and Niu, 2016), DAYCENT (Del Grosso et al., 2000; Nečpálová et al., 2015), and APSIM (Keating et al., 2003;
66 Holzworth et al., 2014), have also included processes to simulate N_2O production, but adopt different parameterizations using
67 static partition parameters to estimate N_2O emission from nitrification, and other empirical parameters to control the influence
68 on nitrification from soil water content, pH, temperature and substrate concentrations. Besides, N_2O is intimately connected

70 with the soil organic carbon (SOC) dynamics, because soil nitrifiers and denitrifiers interact strongly with aerobic and
71 anaerobic heterotrophs that process SOC evolution, and all of these microbes are driven by shared environmental variables
72 including soil temperature, moisture, redox status, and physical and chemical properties (Thornley et al., 2007). As expected,
73 these connections make it difficult for PB models, even the most advanced ones like *ecosys*, to find sufficient representations
74 of the physical and biogeochemical processes or obtain enough data to calibrate a large number of model parameters with
75 strong spatio-temporal variations. Thus, novel approaches are needed for addressing the big challenge of agricultural N₂O flux
76 simulations.

77
78 Machine learning (ML) models can automatically learn patterns and relationships from data. Recent studies have investigated
79 the potential to predict agricultural N₂O emission with ML models, including random forest (RF, Saha et al., 2021),
80 metamodeling with extreme gradient boosting (XGBoost) (Kim et al., 2021), and deep learning neural network (DNN)
81 (Hamrani et al., 2020). Notably, Hamrani et al. (2020) compared nine widely used ML models for predicting agricultural N₂O.
82 That study pointed out that the long short term memory (LSTM) model with recurrent networks containing memory cells as
83 building blocks will be most suitable for N₂O predictions, but the challenge remains with respect to the ability of capturing the
84 sharp peak of N₂O fluxes and lag time between N fertilizer application and the emission peak. Although there is an increasing
85 interest in leveraging recent advances in machine learning, capturing this opportunity requires going beyond the ML
86 limitations, including limited generalizability to out-of-sample scenarios, demand for massive training data, and low
87 interpretability due to the “black-box” use of ML (Karpatne et al., 2017). PB models with their transparent structures built by
88 representations of physical and biogeochemical processes, seem to be exact complementary to ML models. Thus, combining
89 the power of ML model and PB model understanding innovatively is likely a path forward.

90
91 The above need to integrate ML and PB models can be potentially addressed by the newly proposed framework of
92 Knowledge-guided Machine Learning (KGML) models. In the review by Willard et al. (2021), five research frontiers have
93 been identified regarding the development of KGML for diverse disciplines including earth system science, they are: 1) Loss
94 function design according to physical or chemical laws (Jia et al., 2019, 2021; Read et al., 2019); 2) Knowledge-guided
95 initialization through pretraining ML models with synthetic data generated from PB models (Jia et al., 2019, 2021; Read et al.,
96 2019); 3) Architecture design according to causal relations or adding dense layers containing domain knowledge (Khandelwal
97 et al., 2020; Beucler et al., 2019, 2021); 4) Residual modeling with ML models to reduce the bias between PB model outputs
98 and observations (Hanson et al., 2020); and 5) Other hybrid modeling approaches combining PB and ML models (Kraft et al.,
99 2021). These recent advances in KGML pave the pathway to a more efficient, accurate and interpretable solution for estimating
100 N₂O fluxes from the agroecosystem.

101
102 In this study, we present the first-of-its-kind attempt of developing the KGML for agricultural GHG fluxes prediction
103 (KGML-ag) with knowledge-guided initialization and architecture design, and demonstrate the potential of KGML-ag with a

104 case study on quantifying N₂O flux observed by a multi-year mesocosm experiments. We designed the KGML-ag structure
105 based on the causal relations of related N₂O processes informed by an advanced agroecosystem model, *ecosys* (Grant et al.,
106 2003, 2006, 2016). We used the synthetic data generated from *ecosys* to design the KGML-ag input/output, and to pre-train
107 the KGML-ag model to learn the basic patterns of each variable. Observations from multi-season controlled-environment
108 mesocosm chambers (Miller, 2021, thesis; Miller et al., 2021, in review) were used to refine the pretrained KGML-ag and
109 evaluate the model performance. Since there is limited literature that guides the development of KGML-ag and not a one that
110 directly addressed GHG fluxes, we investigated a range of ideas to optimize the model performance, including: 1) Using initial
111 values of intermediate variables (IMVs) instead of sequences as model input to reduce data demand; 2) Building hierarchical
112 structures to explicitly estimate IMVs for further N₂O prediction; 3) Using multitask learning to balance the simultaneous
113 training on multiple variables; and 4) Pretraining with millions of synthetic data generated from *ecosys* and fine tuning with
114 mesocosm observations. Although we evaluated the KGML-ag models with real measurements only from a mesocosm
115 experiment, the lessons learned from the development process and various KGML-ag structures can be transferred to other
116 data, other variables and large scale simulations, therefore have broader implications on further KGML related research in
117 agriculture. We believe this study will stimulate a new body of research on interpretable machine learning for biogeochemistry
118 and other related topics in geoscience.

119 **2 Methods**

120 **2.1 Experimental design overview**

121 To develop and evaluate the KGML-ag models and compare their performance with pure ML models, we designed the
122 following experiments:

- 123 1) With the synthetic data, we developed and pretrained multiple KGML-ag models to learn general patterns and
124 interactions among variables, and evaluated their model performance (Fig. S2, Table 1);
- 125 2) With the observed data, we finetuned multiple KGML-ag models to adapt real-world situations, and evaluated their
126 model performance (Fig. 2-3; Fig. S3-5; Table 2-3);
- 127 3) We further benchmarked KGML-ag models and uncertainties with other pure ML models without considering
128 temporal dependence, including Decision Tree (DT), Random Forest (RF), Gradient Boosting (GB) from the sklearn
129 package (<https://scikit-learn.org/stable/>), Extreme Gradient Boosting (XGB) from the XGBoost package
130 (<https://xgboost.readthedocs.io/en/latest/>) and a 6-linear-layer artificial neural network (ANN) with the mesocosm
131 experiment data by 10 times ensemble experiments (Fig. 4-5; Fig. S6-8);
- 132 4) We conducted a few small experiments to further investigate how various model configurations, such as the
133 pretraining process, data augmentation and IMV initial values would influence KGML-ag model performance (Table
134 3).

135 **2.2 KGML-ag structure development**136 **2.2.1 Generating synthetic data with *ecosys***

137 We generated synthetic data using a PB model, *ecosys*. The *ecosys* model is an advanced agroecosystem model constructed
 138 from detailed biophysical and biogeochemical rules instead of using empirical relations (Grant et al., 2001). It represents N₂O
 139 evolution in the microbe-engaged processes of nitrification-denitrification using substrate kinetics that are sensitive to soil
 140 nitrogen availability, soil temperature, soil moisture, and soil oxygen status (Grant and Pattey 2008). Two groups of microbial
 141 populations, autotrophic nitrifiers and heterotrophic denitrifiers, produce N₂O with specific competitive or cooperative
 142 relations in *ecosys* when O₂ availability fails to meet O₂ demand for their respirations and NO₂⁻ become alternative electron
 143 acceptors. N₂O transfer within soil layers and from soil to the atmosphere is driven by concentration gradient using diffusion-
 144 convection-dispersion equations, in the forms of gaseous and aqueous N₂O under control of volatilization-dissolution (Grant
 145 et al., 2016). Unlike the pipeline model described by Davidson et al. (2000), which mainly consider the correlations of N₂O
 146 production with nitrogen availability and of N₂O emission semionsting with soil water content, *ecosys* enables integrative
 147 effects of energy, water, nitrogen availability on N₂O production and N₂O transfer via the microbial population dynamics and
 148 their interactions with soil, plant, and atmospheric dynamics, under diverse meteorological and anthropogenic disturbances
 149 (e.g. runoff, drainage, tillage, irrigation, soil erosion). Many previous studies have demonstrated its robustness in simulating
 150 agricultural carbon and nitrogen cyclings at different spatial/temporal scales, and under different management practices (Grant
 151 et al., 2003, 2006, 2016; Metivier et al., 2009; Zhou et al., 2021). For the agricultural ecosystems in the US Midwest, whose
 152 simulations are used for synthetic data in this study, the performance of *ecosys* on CO₂ and N₂O fluxes have been extensively
 153 benchmarked, including CO₂ exchange (NEE, R² = 0.87) and leaf area index (LAI, R² = 0.78) from six flux towers, USDA
 154 census reported corn yield (R² = 0.83) and soybean yield (R² = 0.80), satellite-derived GPP for corn (R² = 0.83) and soybean
 155 (R² = 0.85) from Illinois, Iowa and Indiana, and cumulative N₂O emissions (R² = 0.36) across eight Midwestern states (Wang
 156 et al., 2021; Yang et al., 2022). Therefore, *ecosys* is an appropriate choice of domain knowledge provider and synthetic data
 157 generator in the development of KGML models. We generated daily synthetic data including N₂O flux and 76 IMVs (e.g. CO₂
 158 flux from soil, layerwise soil NO₃⁻ concentration, layerwise soil temperature, and layerwise soil moisture; detailed in Table
 159 S1) from *ecosys* simulations for 2000-2018 over 99 randomly selected counties in Iowa, Illinois, and Indiana, USA. We used
 160 hourly meteorological inputs (downward shortwave radiation, air temperature, precipitation, relative humidity, and wind
 161 speed) from the phase 2 of North American Land Data Assimilation System (NLDAS-2, Xia et al., 2012) and layerwise soil
 162 properties (e.g. bulk density, texture, pH, SOC concentration) from the SSURGO database (Soil Survey Staff, 2020) as inputs
 163 to *ecosys*. Crop management except N fertilization rates were configured to the same settings as mesocosm experiments
 164 (described in Sec 2.2.2). To increase the variability in synthetic data, we implemented 20 different N fertilization rates ranging
 165 from 0 to 33.6 g N m⁻² (i.e. 0 to 300 lb N ac⁻¹) in each simulation of 99 counties, and more detailed information for model
 166 setup refers to Zhou et al. (2021).

Commented [1]: Grant, R. F., & Pattey, E. (2008). Temperature sensitivity of N₂O emissions from fertilized agricultural soils: Mathematical modeling in *ecosys*. *Global Biogeochemical Cycles*, 22(4). <https://doi.org/10.1029/2008gb003273>
 Grant, R. F., Neftel, A., & Calanca, P. Ecological Controls on N₂O Emission in Surface Litter and Near-surface Soil of a Managed Pasture: Modelling and Measurements. *Biogeosciences* 13 3549–71

Commented [2R1]: Hi Yufeng, we expect a little more details of the similarity and differences between *ecosys* model and the pipe line model (like what mentioned in figure 2, Davidson et al., 2000, <https://academic.oup.com/bioscience/article/50/8/667/243260>) of N₂O simulation. I remember your previous version of manuscript (https://docs.google.com/document/d/1KbQngIvd_pFfPccI5eq592fKzbSVyL5mOVciSwmq8/edit?usp=sharing) section 2.1 para2 has very detailed description of *ecosys* model N₂O part.

Here could you help us 1) briefly check Davidson et al., 2000 N₂O pipe line model and 2) compare with *ecosys* model to find the similarity and differences? (like something I intuitively think, a) *ecosys* comprehensively calculated some parts ...

Commented [3R1]: I added those general descriptions on *ecosys* N₂O emissions. I've provided more details as needed and comparisons with the pipe model

Commented [4]: @yang6956@umn.edu Hi Yufeng, I may need your help here adding few sentences to 1) Explain the *ecosys* model structure of simulating N₂O and the differences between simple pipeline model ; 2) *ecosys* model performance on various ecosystem for CO₂/N₂O. You should have pretty enough materials before from your paper for thi...
 ...

Commented [5R4]: Original related review comments:

Robustness of physical (prior) knowledge

ecosys model plays a central role in guiding the ML model i...

Commented [6R4]: Moreover, Wang has summarized few previous model simulation comparisons with field level observations here, in case you need (https://docs.google.com/document/d/1tRTQi7R-mCwMN_uqT-5klski8cNad-Rs0Umeffk0uU/edit?usp=sharing). In the maintext we may...

Commented [7]: A problem here with *ecosys* N₂O studies is that R₂ or other quantitatives are missing in daily N₂O flux comparison

Commented [8R7]: Hi Yufeng, is there a way to cite your paper in current stage? if yes please provide the detailed citation, thanks @yang6956@umn.edu

Commented [9R7]: Yang, Y., Liu, L., Zhou, W., Guan, K., Kim, T., Tang, J., Peng, B., Zhu, P., Grant, R. F., Griffis, T. J., Jin, Z. (2022). Distinct driving mechanisms of non-growing season N₂O emissions call for spatial-specific mitigation strategies in the US Midwest. *One Earth*. Submitted. Is it proper to provide the journal name directly as just ...

167

168 The generated synthetic data were then processed for further use by KGML-ag development. Meanwhile, the hourly weather
 169 forcings were converted to seven daily variables, including the maximum air temperature (TMAX_AIR, °C), difference
 170 between the maximum and the minimum air temperature (TDIF_AIR, °C), the maximum humidity (HMAX_AIR, fraction),
 171 difference between the maximum and the minimum humidity (HDIF_AIR, fraction), surface downward shortwave radiation
 172 (RADN, W m⁻²), precipitation (PREC, mm day⁻¹), and wind speed (WIND, m s⁻¹). Six soil properties were retrieved from the
 173 SSURGO database, including total averaged (depth weighted averaged for all layers) bulk density (TBKDS, Mg m⁻³), sand
 174 content (TCSAND, g kg⁻¹), silt content (TCSILT, g kg⁻¹), pH (TPH), cation exchange capacity (TCEC, cmol⁺ kg⁻¹) and soil
 175 organic carbon (TSOC, g C kg⁻¹); and two crop properties were retrieved, including planting day of the year (PDOY) and crop
 176 type (CROPT, 1 for corn and 0 for soybean). Finally, each synthetic data sample has daily N₂O flux, 76 selected IMVs, 7
 177 weather forcings (W), 1 N fertilization rate (FN, g N m⁻²) and 8 soil/crop properties (SCP) (Fig. 1.a; Table S1). The periods
 178 from April 1st to July 31st (122 days) were selected to cover the mesocosm observations (around 30 days before and 90 days
 179 after N fertilizer date). The total amount of synthetic data sample is 122 days x 18 years x 99 counties x 20 N fertilizer rates
 180 (about 4.3 million data points). We randomly selected the samples from 70 counties for training, 10 counties for validation,
 181 and 19 counties for testing.

182 **2.2.2 Mesocosm experiments for KGML-ag model fine-tuning and evaluation**

183 Observations were acquired from a controlled-environment mesocosm facility on the St. Paul campus of the University of
 184 Minnesota. Soil samples were sourced in 2015 from a farm in Goodhue County, MN (44.2339° N and 92.8976° W), which had
 185 been under corn-soybean rotation for 25 years. Six chambers with a soil surface area of 2 m² and column depth of 1.1 m were
 186 used to plant continuous corn during 2015-2018 and monitor the N₂O flux response to different precipitation treatments. The
 187 experiment also measured other environmental variables including air temperature and photosynthetically active radiation
 188 (PAR), which were controlled to mimic the outdoor ambient environment. Granular urea fertilizer was hand broadcasted and
 189 incorporated to a depth of 0.05 m to each chamber at a rate of 22.4 g N m⁻² (200 lb N ac⁻¹) on May 1st of 2015, May 4th of
 190 2016 and May 3rd of 2017, and 10.3 g N m⁻² (92 lb N ac⁻¹) on May 8th of 2018. Corn hybrid (DKC-53-56RIB) were hand
 191 planted to a depth of 0.05 m in two rows spaced 0.76 m apart 3-5 days after fertilizer application, at a seeding rate of 35,000
 192 seeds ac⁻¹ in 2015 to 2017, and 70,000 seeds ac⁻¹ in 2018 but thinned upon emergence to ensure 100 percent emergence at
 193 35,000 seeds ac⁻¹. Crops were harvested at the end of September by cutting the stover five inches above the soil. Hourly N₂O
 194 fluxes (mg N m⁻² h⁻¹) and CO₂ fluxes (g C m⁻² h⁻¹) were measured using non-steady-state flux chambers with a CO₂ analyzer
 195 (LI-10820 for 2016 and LI-7000 for 2017 and 2018, LI-COR Biosciences, Lincoln, NE) and a N₂O analyzer (Teledyne
 196 M320EU, Teledyne Technologies International Corp, Thousand Oaks, CA) (Detail method can be retrieved from Fassbinder
 197 et al., 2012, 2013). We also collected soil moisture at 15 cm depth (VWC as abbreviation of volumetric water content, m³ m⁻³),
 198 weekly 0-15 cm depth soil NO₃⁻ + NO₂⁻ concentration (NO₃⁻ for short in the following text, g N Mg⁻¹), soil NH₄⁺
 199 concentration (NH₄⁺, g N Mg⁻¹), and related environment variables including air temperature, radiation, humidity and soil/crop

200 properties from three growing seasons during 2016-2018 and six mesocosm chambers (Fig. S1). [The magnitude of N₂O flux](#)
201 [and NO₃⁻ soil concentration and their responses following fertilizer application from this mesocosm experiment are consistent](#)
202 [with several field studies of agricultural soils \(Fassbinder et al., 2013; Grant et al., 1999, 2006, 2008; Hamrani et al., 2020;](#)
203 [Venterea et al., 2011\)](#) More details about the mesocosm facility and experimental design can be found in the thesis of Miller
204 L. (2021).

205
206 The observed data were then processed to fine-tune and evaluate the KGML-ag models. The N₂O flux and four IMVs and
207 weather variables were collected from the measurements in the selected period (i.e., April 1st to July 31st). Weekly NO₃⁻ (short
208 for soil NO₃⁻ within 0-15 cm depth), and NH₄⁺ (short for soil NH₄⁺ within 0-15 cm) were linearly interpolated to the daily time
209 scale on days containing VWC (short for soil VWC in 15 cm) data. Hourly air temperature, net radiation, N₂O (short for N₂O
210 fluxes from soil), CO₂ (short for CO₂ fluxes from soil) and VWC were resampled to daily scale. All SCP were derived from
211 mesocosm measurements except that TCEC was derived from the SSURGO database according to the soil origin. We used the
212 leave-one-out cross-validation (LOOCV) method for the finetuning and evaluation process. Each time we used one chamber
213 data for validation and another five chambers' data for model finetuning.

214
215 [To increase the model generalization and avoid overfitting, we used the data augmentation method to enrich the finetuning](#)
216 [data set to be 1000 times larger. Data augmentation is a typical practice in ML when training data is limited \(Meyer et al.,](#)
217 [2021\). In particular, we randomly sampled 16 hours of data from a 24 hours period in each day and chamber, and then used](#)
218 [the sampled data to calculate the daily value. If less than 16 missing values existed in 24 hours, we used the above method to](#)
219 [sample the data and calculated a fraction number \(24 missing value number\)/24 to record valid data fraction in the mask](#)
220 [matrix. If more than 16 missing values were found, we dropped this point and recorded 0 in the mask matrix. The final sample](#)
221 [has daily N₂O flux, 4 IMVs, 7 weather forcing variables and 8 static soil/crop properties \(similar to synthetic data\). The total](#)
222 [amount of augmented observed data sample is 122 days x 3 years x 6 chambers x 1000 data augmentations. The mask matrix](#)
223 [is of the same size as the observed data sample but its elements range from 0 to 1.](#)

224
225 [To reduce overfitting and increase the generalization of the trained model based on the small amount of mesocosm](#)
226 [data, we applied the following method to augment the experimental measurements and weather forcings to 1000](#)
227 [times larger by sampling hourly data and averaging them to daily scale. In this method, 16 hours \(or maximum](#)
228 [valid hours\) of data are randomly selected from 24 hours of data to compute their mean as the daily value. Since](#)
229 [3/4 of the day are covered by the selected data \(16 hours /24 hours\), the augmented daily values should be](#)
230 [representative enough for the source day and meanwhile present slight variations. Furthermore, the observation](#)
231 [ratio, \(24 hours - missing hours\) / 24 hours, can be used as the weights in loss function to inject the data quality](#)
232 [information in model optimization. If the day has more than 16 hours missing values, we consider the observations](#)

Commented [10]: @xu000114@umn.edu Hi Shaoming, I
may need your help here to clarify the data augmentation
method. You may modify this part as many as you want but
with a track. The basic strategy is to answer the three
questions from Referee#2. The related comments list below:

**recommend that the paragraph starting at line 194 be
rewritten for clarity. First, data augmentation is a class of
methods, not a single method. Second, Meyer et al. use
copula-based models in particular to augment datasets. Do
you use copula-based methods? The way this reference is
cited suggests that you follow their approach. Third, do you
randomly sample observed data, or synthetically generated
data, or both? Do you randomly sample only the data which
are hourly, e.g., air temperature, net radiation, N₂O, CO₂, and
VWC? How is the daily value calculated from the sampled
data? I did not find the answers to these questions to be clear
from the text.

Assigned to Shaoming Xu

233 in that day as not trustworthy and drop the day by setting the weight to 0. This method can not only augment the
234 data to 1000 times larger but also deal with the missing values in observed data inherently. The total amount of
235 observed mesocosm data and related weather forcings are augmented to 122 days x 3 years x 6 chambers x 1000
236 data samples in this study.]

Commented [11]: Please check if this paragraph is well fit
your needs to replace the previous paragraph.
@lichengl@umn.edu

238 2.2.3 Gated Recurrent Unit (GRU) as the basis of KGML-ag

239 Hamrani et al. (2020) compared different models and reported that LSTM provided the highest accuracy in predicting N₂O
240 fluxes, because N₂O flux is time dependent by its production/consumption nature and LSTM simulates target variablesvariable
241 by considering both current and historical states. The LSTM model, proposed by Hochreiter and Schmidhuber (1997), uses a
242 cell state as an internal memory to preserve the historical information. At each time step, it creates a set of gating variables to
243 filter the input and historical information and then uses the processed data to update the cell state. Similar to LSTM, GRU is a
244 gated recurrent neural network but only keeps one hidden state (Cho et al., 2014). Though simpler than LSTM, GRU is proved
245 to have similar performance (Chung et al., 2014). Our preliminary test on synthetic data for N₂O prediction showed that GRU
246 indeed provided similar or higher accuracy and model efficiency under different model settings than LSTM (Table S2). This
247 is possiblelikely because simpler models with fewer weights and hyperparameters are more robust in combating the overfitting
248 problem. Therefore, we choose GRU as the basis of KGML-ag development.

249 2.2.4 Incorporating domain knowledge to the development of KGML-ag

250 To quantitatively reveal the correlations between N₂O fluxes and IMVs and guide the KGML-ag development, we conducted
251 the-feature importance analysis by a customized 4-layer GRU ML model (Fig. 1b). Each layer of the model has a GRU cell
252 with 64 hidden units. The 4-layer structure makes the model deeper and capable of capturing complex interactions. Between
253 each GRU cell, 20% of the output hidden states are randomly dropped by replacing them with zero values (so called 20%
254 dropout) to avoid overfitting. A linear dense layer is used to map the final output to N₂O. We first trained GRU models usingby
255 synthetic data with different combinations of IMVs as inputs to predict the N₂O fluxes (original-test, Table S2). The feature
256 importance analysis of well-trained models was then implemented by replacing one input feature with a Gaussian noise with
257 mean $\mu=0$ and standard deviation $\sigma=0.01$, while keeping others untouched (new-test). The importance score was calculated by
258 the new-test's root mean square error (RMSE) (replacing one feature) minus the original-test's RMSE (no replacing). RMSE
259 was calculated by $\sqrt{\frac{\sum_{i=1}^N (y_i - y_i')^2}{N}}$ where N is the total number of observations across time and space, y_i is i-th measurement
260 from synthetic data or observed data and y_i' is its corresponding prediction.

262 To find important variables for N_2O flux prediction in an ideal situation wherethat all variables are available, we conducted a
263 feature importance analysis for GRU models with all IMVs and basic inputs including FN, 7 W and 8 SCP (Fig. S2a). Results
264 indicated that flux variables including NH_3 , H_2 , N_2 , O_2 , CH_4 , evapotranspiration (ET) and CO_2 had significant influence on the
265 model performance. Variables ranked high in feature importance analysis are should be primarily considered with priority
266 during model development. To develop a functional KGML-ag in real world, we further investigated the feature importance
267 of four IMVs that are available from mesocosm observations including CO_2 , NO_3^- , VWC and NH_4^+ , which were ranked 7th,
268 20th, 58th, 60th respectively in 92 input features of synthetic data (Fig. S2a). We used these four available IMVs to create two
269 input combinations: 1) CO_2 flux, NO_3^- , VWC and NH_4^+ (IMVcb1), and 2) NO_3^- , VWC and NH_4^+ (IMVcb2). The objective of
270 building IMVcb2 was to investigate the importance of highly ranked variable CO_2 flux (by removing it from the inputs), and
271 the impact of mixing-up flux and non-flux variables on model performance. We tested the feature importance of the GRU
272 models built with IMVcb1 and IMVcb2 to check whether they would help in N_2O prediction (Fig. S2b-c). All the feature
273 importance results above indicated the correlation intensity between N_2O and many other variables, which would help the
274 KGML-ag model development and interpretation in this study (rest of this section and Sec. 3.1), and would guide future N_2O
275 related measurements and KGML model development (discussed in Sec. 4.34).
276

277 Next we used the knowledge learned from synthetic data to develop the structure of KGML-ag (Fig. 1cb-de). Previous studies
278 for KGML models have used physical laws, e.g., conservation of mass or energy, to design the loss function for constraining
279 the ML model to produce physically consistent results (Read et al., 2019; Khandelwal et al., 2020). However, for complex
280 systems like agroecosystems, it is challenging to incorporate physical laws, such as mass balance for N_2O , into the loss function
281 due to the incomplete understanding of the processes and the lack of mass balance related data for validation. An alternative
282 solution is to incorporate such information in the design of the neural network (Willard et al., 2021). Effectiveness of such an
283 approach was demonstrated by Khandelwal et al. (2020) in the context of modeling stream flow in a river basin using Soil &
284 Water Assessment Tool (SWAT). They used a hierarchical neural network to explicitly model IMVs (e.g., soil moisture, snow
285 cover) and their relationships with the target variable (streamflow) and showed that this model is much more effective than a
286 neural network that attempts to directly learn the relationship between input drivers and the target variables. Following this
287 idea, we identified four desired features of an effective KGML-ag model, including: 1) We used initial values instead of
288 sequence of the IMVs from synthetic data or observed data to provide a solid starting state for the ML system and reduce the
289 IMV data demand, and then used the rest of the data to further constrain the prediction of IMVs; 2) We built a hierarchical
290 structure based on the structure of process representation in causal relations derived from ecosys to first predict IMVs and then
291 simulate N_2O with predicted IMVs; 3) We trained all variables together using multitask learning to reach the best prediction
292 scores, which generalized the model and incorporated interactions between IMVs and N_2O ; 4) We initialized the KGML-ag
293 model by pretraining with using synthetic data before using real observed data to transfer physical knowledge, which further
294 reduced the demand on large training samples and aided in faster convergence for fine-tuning.

295

296 To meet these desired features, we proposed two KGML-ag models (Fig. 1c-d). The first model, KGML-ag1, is a hierarchical
 297 structure containing two modules to simulate IMVs and N₂O sequentially. Each module is a 2-layer 64 units GRU ML model.
 298 The inputs to the module of the KGML-ag1 model for IMV predictions (KGML-ag1-IMV module) are FN, 7W and 8SCP
 299 together with the initial values of IMVs, and the outputs are IMV predictions. The inputs to the module of the KGML-ag1
 300 model for N₂O predictions (KGML-ag1-N₂O module) are FN, 7W, 8SCP and predicted IMVs from KGML-ag1-IMV, and the
 301 output is the target variable N₂O. Linear dense layers were coded for both modules to map output states to IMVs or N₂O. The
 302 dropout method was applied to drop 20% of the state output between GRU cells and dense layers. The second model, KGML-
 303 ag2, is also a hierarchical structure similar to KGML-ag1, but has multiple KGML-ag2-IMV modules to explicitly simulate
 304 IMVs by tuning them separately in the fine-tuning process (discussed in Sec. 2.2.5). Each KGML-ag2-IMV module in KGML-
 305 ag2 is a 2-layer 64 units GRU cell with the inputs of FN+7W+8SCP and one IMV initial value, and the output of one IMV
 306 prediction. The KGML-ag2-N₂O module collects the IMV predictions from KGML-ag2-IMV modules and predicts the N₂O
 307 with inputs of FN+7W+8SCP and predicted IMVs.

308 2.2.5 Strategies for pretraining and fine-tuning processes

309 To increase the efficiency of the training process, we used the Z-normalization ($\frac{(X - \mu)}{\sigma}$, where X is the vector of a particular
 310 variable over all the data samples in the data set; μ is the mean value of X ; σ is the standard deviation of X) method to normalize
 311 each variable separately on synthetic data. Then the scaling factors (μ, σ) derived from *ecosys* synthetic data for each variable
 312 were used to Z-normalize observed data into the same ranges as synthetic data. As mentioned in Sec. 2.2.1, the TDIF_AIR,
 313 HDIF_AIR were used instead of absolute min temperature (TMIN_AIR) and humidity (HMIN_AIR). This is done because
 314 TMIN_AIR and HMIN_AIR follow similar trends as TMAX_AIR and HMAX_AIR, making Z-normalization numerically
 315 poorly defined. Using the difference between maximum and minimum can provide a clearer information of daily air
 316 temperature/humidity variation.

317

318 During the pretraining process, we initialized the IMV of KGML-ag using the first day value of synthetic IMV time series.
 319 Adam optimizer with a start learning rate of 0.0001 was used for the training process. The learning rate would decay by 0.5
 320 times after every 600 training epochs. At each epoch, synthetic data samples were randomly shuffled before being input to the
 321 model to predict N₂O (and IMVs if any). The mean square error (MSE) loss (calculation was equal to the square of RMSE) or
 322 sum of MSE loss (if multitask learning) between predictions and *ecosys* synthetic observations were calculated to optimize the
 323 weights of GRU cells. After the training process updated the model's weights, the validation process was performed to evaluate
 324 the model performance based on untouched samples with RMSE and the square of Pearson correlation coefficient (r^2). r^2 was
 325 calculated as $\frac{\sum_i (y_i' - \bar{y}_i')(y_i - \bar{y}_i)^2}{\sum_i (y_i' - \bar{y}_i')^2(y_i - \bar{y}_i)^2}$, where y_i is the i-th measurement from synthetic data or observed data, y_i' is its

326 corresponding prediction, \underline{y}_i is the mean of the measurement y in diagnosing space and \underline{y}'_i is the mean of the predicted y' in
327 diagnosing space. If both validated r^2 and RMSE were better than the best values in previous epochs, the updated model in this
328 epoch would be saved. Normalized RMSE (NRMSE, calculated by RMSE/(max-min) of each variable observation) was
329 introduced to evaluate IMV predictions between variables with different value ranges.

330
331 During the fine-tuning process, we used estimated IMV initial values of 1.0 g C m^{-2} , $0.2 \text{ m}^3 \text{ m}^{-3}$, 0.0 g N Mg^{-1} , and 20.0 g N
332 Mg^{-1} for CO_2 , VWC, NH_4^+ , and NO_3^- respectively, from starting day (April 1st) to the day before the first day of real
333 observations, as input to KGML-ag models. Then the first-day values of observed IMVs were input into KGML-ag during the
334 rest days of the period as IMV initial values. In addition, as described in Sec. 2.2.2, we used a data augmentation method to
335 augment the total amount of data 1000 times larger for the fine-tuning process. The purpose of this data augmentation method
336 was to increase the generalization of the fine-tuned model and to overcome the overfitting due to small sample size. The mask
337 matrix was elementarily multiplied to the output matrix to calculate the MSE, r^2 and RMSE only for days with observations.
338 The similar optimizer was used with an initial learning rate of 0.00005 and decay fraction of 0.5 per 200 epochs. Other
339 training/validation methods in each epoch were similar to the pretraining process. Specifically, in the KGML-ag1 model
340 finetuning process, we first froze the KGML-ag1- N_2O module and only trained the KGML-ag1-IMV module for IMVs. After
341 finishing the KGML-ag1-IMV module training, we froze the KGML-ag1-IMV module and trained the KGML-ag1- N_2O
342 module for N_2O . In the KGML-ag2 fine-tuning process, the similar freezing method was used but different KGML-ag2-IMV
343 modules were trained separately one by one.

344 2.3 Development environment description

345 We used the Pytorch 1.6.0 (<https://pytorch.org/get-started/previous-versions/>) and python 3.7.9
346 (<https://www.python.org/downloads/release/python-379/>) as the programing environment for the model development. In order
347 to use the GPU to speed-up the training process, we installed cudatoolkit 10.2.89 (<https://developer.nvidia.com/cuda-toolkit>).
348 A desktop with Nvidia 2080 super GPU was used for code development and testing. The Mangi cluster
349 (<https://www.msi.umn.edu/mangi>) from High Performance Computing of Minnesota Supercomputing Institute (HPC-MSI,
350 <https://www.msi.umn.edu/content/hpc>) with 2-way Nvidia Tesla V100 GPU was used in training processes which consumed
351 longer time and bigger memories.

352 3 Results

353 3.1 Pretraining experiments using synthetic data from *ecosys*

354 In the pretraining stage, the GRU model with 76 IMVs achieved the best performance in predicting N_2O fluxes ($r^2=0.98$, RMSE
355 $=0.54 \text{ mg N m}^{-2} \text{ day}^{-1}$ and normalized RMSE (NRMSE) $= 0.01$) on the test set of synthetic data generated from *ecosys* (Table

356 1). The high performance was due to some flux IMVs such as NH₃, H₂, O₂, CO₂ and ET, which are highly correlated to N₂O
357 (Fig. S2a), were used as input to the model. The good performance of GRU with all IMVs indicates that ML models are able
358 to perfectly mimic *ecosys* when sufficient information about IMVs is available. The GRU model with only basic input of N
359 fertilizer rate, 7 weather forcings, and 8 soil/crop properties (FN+7W+8SCP) had the accuracy of $r^2=0.89$ and RMSE = 1.37
360 mg N m⁻² day⁻¹ (Table 1). The relatively low performance is likely because this model failed to capture several highly nonlinear
361 pathways that are employed by *ecosys* to predict N₂O (e.g., one influence pathway from precipitation to N₂O can be:
362 Precipitation → soil moisture → N components solubility/concentration → nitrification/denitrification rate/amount → soil
363 N₂O concentration → gas N₂O flux). When adding sequences of IMV combinations (i.e., IMVcb1 of CO₂ flux, NO₃⁻, NH₄⁺
364 and VWC, and IMVcb2 of NO₃⁻, NH₄⁺ and VWC), the GRU models performed slightly better than the GRU model using only
365 basic inputs, achieving r^2 of 0.92 and 0.90, respectively (Table 1). The KGML-ag1 with IMVcb1 and IMVcb2 initial values
366 provided better performance (both $r^2 = 0.90$) than GRU with basic input and comparable performance to the GRU with inputs
367 of IMVcb1 and IMVcb2 sequence. Besides, KGML-ag1 provided predicted IMVs of CO₂, NO₃⁻, NH₄⁺, and VWC with r^2 over
368 0.91, and NRMSE below 0.06 (Table 1). KGML-ag2 also provided comparable N₂O performance but relatively better IMVs
369 performance of r^2 over 0.92 and NRMSE below 0.05. Results indicated that KGML-ag models with IMV initial values as extra
370 input performed similar or better than pure ML models in synthetic data.

371 3.2 KGML-ag evaluation using observed data from mesocosm

372 After being fine-tuned with observed data, KGML-ag1 had N₂O prediction overall accuracy of $r^2=0.81$ and RMSE=3.6 mg N
373 m⁻² day⁻¹, while non-pretrained GRU model provided $r^2=0.78$ and RMSE=4.0 mg N m⁻² day⁻¹, and pretrained GRU model
374 provided $r^2=0.80$ and RMSE=3.77 mg N m⁻² day⁻¹ (Table 3). The time series of N₂O predictions from KGML-ag1 and the non-
375 pretrained GRU model were further compared (Fig. 2), from which we found at least two advantages of using KGML-ag1 for
376 N₂O predictions: 1) For the region without observation data (normally before day 25), KGML-ag1 predicted stable N₂O fluxes
377 close to 0 mg N m⁻² day⁻¹ (which is close to the reality in the experiment setting) while GRU caused anomalous peaks of fluxes.
378 This is because KGML-ag1 has learned knowledge “common sense” for the whole period from the pretraining process with
379 *ecosys* model generated synthetic data, but GRU model has no prior knowledge for the period without any data in observations;
380 2) Although KGML-ag1 had a lower accuracy than GRU in some chambers, KGML-ag1 can better capture the temporal
381 dynamics of N₂O fluxes compare to GRU, especially when the fluxes are highly variable (e.g. Fig 2 chamber 2).

382 To validate KGML-ag1 robustness, we further investigated the KGML-ag1 and GRU model performance in different temporal
383 windows, shrinking from the whole period to the N₂O peak occurrence time (days 1-122, day 30-80, day 40-65 and day 45-60
384 for year 2016-2018), and performance in N₂O flux, first order gradient of N₂O (slope) and second order gradient of the N₂O
385 (curvature) (Table 2). Slope represents the speed of N₂O flux changes through time and curvature represents the acceleration.
386 Assessing prediction performance within these two metrics will reveal the model robustness on capture variable dynamics.

388 which is critical when predicting fast-change variables with hot moments like N₂O. First of all, the overall r^2 and RMSE of
389 KGML-ag1 for values, slope and curvature were always better than GRU. In particular, KGML-ag1 captured the peak region
390 (e.g., days 45-60) much better than GRU in both magnitude and dynamics (Table 2, Fig 2). Even for chamber 2 and 5 in
391 which KGML-ag1 made worse N₂O predictions than GRU (Δr^2 ranging from -0.07 to -0.03), it better captured temporal
392 dynamics than GRU in terms of slope (Δr^2 ranging from 0.08 to 0.16) and curvature (Δr^2 from 0.11 to 0.23) (Table 2). For other
393 chambers, KGML-ag1 outperformed GRU consistently. For chamber 1, KGML-ag1 had worse N₂O predictions RMSE than
394 GRU but the Δr^2 increased as the window shrinks to the peak emission time (0.07 → 0.13). The slope and curvature for
395 chamber 1 also indicated that KGML-ag1 captured the dynamics much better than GRU. For chamber 3, KGML-ag1
396 predicted better N₂O but presented worse slope and curvature RMSE than GRU (Table 2). However, when explicitly
397 investigating the time series of N₂O flux, slope and curvature in each year, KGML-ag1 outperformed GRU more significantly
398 in 2017, the year with more complex temporal dynamics of N₂O fluxes, than in 2016 and 2018, especially for chamber 3 (Fig.
399 2; Fig. S3-4). This investigation supported that KGML-ag1 was more capable for complex dynamics predictions.
400

401 Interestingly, the fine-tuned KGML-ag1 model predicted reasonable IMVs including CO₂, NO₃⁻, NH₄⁺, and VWC with overall
402 r^2 of 0.37, 0.39, 0.60, and 0.33 and NRMSE of 0.14, 0.21, 0.09 and 0.18, respectively (Table 3). The time series comparisons
403 between IMV predictions and observations further indicated that KGML-ag1 could reasonably capture both magnitude and
404 dynamics (Fig. 3). KGML-ag2 presented better IMVs predictions than KGML-ag1, with overall r^2 of CO₂, NO₃⁻, NH₄⁺, and
405 VWC increasing by 0.37, 0.17, 0.06 and 0.51, and NRMSE decreasing by 0.05, 0.03, 0.01 and 0.10, respectively, but a slightly
406 lower r^2 (decreasing 0.02) of N₂O (Table 3; Fig. S5). This indicated that explicitly simulating each IMV with separated KGML-
407 ag2-IMV modules did not benefit the N₂O flux prediction accuracy, likely due to increasing model complexity which resulted
408 in reduced stability and ignoring the IMV interactions. In addition, we also found all KGML-ag models would perform
409 better by using IMVcb1 (with CO₂) than using IMVcb2 (without CO₂) in real data tests, indicating feature importance analysis
410 based on synthetic data can be a reasonable substitute for analysis with the often limited real-world data.

Commented [12]: model stability?

Commented [13R12]: Yes the model stability will be reduced due to more parameters in ML models to be determined in KGML-ag2.

411 3.3 KGML-ag comparing with other pure ML models

412 The results from eightseven different models showed that KGML-ag1 comparing with other pure ML models consistently
413 provided the lowest RMSE (3.59-3.9460 mg N m⁻² day⁻¹, 1.14-1.2320 mg N m⁻² day⁻², and 0.84-0.897 mg N m⁻² day⁻³) and
414 highest r^2 (0.78-0.81, 0.48-0.5654, and 0.23-0.318) for N₂O fluxes, slope and curvature, respectively (Fig. 4). This indicated
415 that KGML-ag1 outperformed other pure ML models in both capturing both the magnitude and dynamics of N₂O flux. KGML-
416 ag2 presented slightly better mean scores for N₂O flux predictions than KGML-ag1, but worse scores for slope and curvature
417 and larger uncertainties. This proved the hypothesis discussed in section 3.2 that KGML-ag2 didn't benefit the magnitude and
418 dynamics predictions of N₂O flux with its more complex structure and less connections between IMVs.
419

420 Within the tree-based models (DT, RF, GB and XGB), the simplest model DT provided the worst predictions for N₂O flux,
421 slope and curvature. The XGB model provided the highest N₂O flux accuracy with r^2 of 0.61-0.632 and RMSE of 5.07-5.1744
422 mg N m⁻² day⁻¹, while the GB model provided best slope and curvature predictions with r^2 of 0.38-0.4042 and 0.23-0.268, and
423 RMSE of 1.34-1.374 mg N m⁻² day⁻² and 0.91-0.9588 mg N m⁻² day⁻³, respectively. The highest N₂O flux accuracy and
424 relatively low slope and curvature accuracy of the XGB model implied that there is a trade-off between the abilities of capturing
425 dynamics and magnitude.

426

427 In the group of deep learning models including ANN, GRU and KGML-ag1, ANN provided the worst predictions. Even with
428 the better N₂O flux predictions than most tree-based models (except XGB), the slope and curvature predictions of ANN were
429 the worst among all eightseven models. This implied that the trade-off between accurately capturing N₂O dynamics to
430 magnitude in ANN was significant. But when considering the temporal dependence, deep learning model GRU and KGML-
431 ag1 outperformed all other models in flux, slope and curvature predictions. This indicated that without considering temporal
432 dependence the improvement in N₂O flux prediction accuracy could be risky by causing the performance drop in capturing
433 dynamics.

434

435 The detailed model comparisons in each chamber are shown in Fig. 5 (N₂O flux) and Fig. S6-7 (N₂O slope and curvature),
436 where the results are found to follow the same pattern as described above. In addition, time series comparisons of chamber 3
437 and 4 in 2017 between different models are presented in Fig. S8 as two examples. From these comparisons, we infer that
438 without considering temporal dependence and pretraining process, the tree-based model including DT, RF, GB and XGB and
439 deep learning model ANN predicted erratic peaks in almost every missing data point, while GRU model was stable in small
440 gaps and only presented poor performance in long missing period (before 25 day). This improvement by GRU model can be
441 attributed to the structure of GRU that naturally keeps the historical information using hidden states, which enables GRU to
442 consider the temporal dependence and make consistent predictions over time.

443 **3.4 Influence of pretraining process, data augmentation and using IMV initial values as input feature**

444 After we pretrained the GRU model with synthetic data, the overall r^2 of N₂O flux predictions in observed data increased by
445 0.02, 0.12 and 0.14, and RMSE decreased by 0.23 mg N m⁻² day⁻¹, 0.15 mg N m⁻² day⁻² and 0.02 mg N m⁻² day⁻³ for flux, slope
446 and curvature predictions, respectively, compared to non-pretrained GRU (Table 3 gray region). The gap between the GRU
447 model with pretrain and KGML-ag1 in N₂O value prediction shows the improvement resulting from architecture change (r^2
448 increases by 0.01 and RMSE decreases by 0.17 mg N m⁻² day⁻¹). Although pretrained GRU had higher slope and curvature
449 prediction accuracy than KGML-ag models, it still couldn't achieve the current N₂O value prediction accuracy of KGML-ag1.
450 Besides, the KGML-ag models had relatively shallow N₂O prediction modules (2-layer GRU KGML-ag-N₂O module of
451 KGML-ag models vs 4-layer GRU) but included modules for IMV predictions, which therefore increased the model
452 interpretability.

453

454 It's worth noting that prediction accuracy of all KGML-ag models dropped without augmenting the training dataset in the fine-tuning process (Table 3 blue region). Moreover, the maximum training epochs increased from 800 to 20000, which resulted in overfitting on the small data set. This indicated that the data augmentation indeed helped the models become more generalizable and gain better accuracy.

458

459 Experiments using zero initial values presented a significant drop in every variable's prediction accuracy (Table 3 yellow region). This indicated that the IMV initial values input into the KGML-ag-IMV modules of KGML-ag models influenced not only the IMV prediction but also the N₂O prediction of the KGML-ag-N₂O module. This shows that there is useful information transferred from IMVs in the KGML-ag-IMV module to the KGML-ag-N₂O module.

463 4 Discussion

464 In the previous section, we showed that KGML-ag models can outperform ML models, by invoking architectural constraints and PB model synthetic data initialization. Compared to traditional PB models such as *ecosys*, KGML-ag models provide computationally more accurate and efficient predictions (KGML-ag few seconds vs *ecosys* half hour), which is similar to traditional ML surrogate models (Fig. S9). But KGML-ag goes beyond that by providing more interpretable predictions than pure ML models.

469 4.1 Interpretability of KGML-ag

470 The proposed KGML-ag models incorporate causal relations among N₂O related variables/processes as shown in Fig. S10. 471 Managements, weather forcings and initial values of IMVs influence soil water, soil temperature and soil properties, which 472 influence the availability of O₂ and N as well as the microbe populations in soil, and further influence the nitrification and 473 denitrification rates. N₂O is produced during both nitrification and denitrification when soil O₂ concentration is limited. Our 474 KGML-ag follows this hierarchical structure by designing KGML-ag-IMV modules representing the soil processes for IMVs 475 predictions (Fig. 1c-d).

476

477 To better explain the time series predictions of N₂O flux (Fig. S1; Fig. 2-3), we separated the observations of each year into 478 three periods: leading period (before N₂O increasing), increasing period (increasing to the peak) and decreasing period (peak 479 decreasing to near zero). During the leading period, both NH₄⁺ and CO₂ were increasing immediately in the following few days 480 following urea N fertilizer application, indicating that urea was decomposing into NH₄⁺ and CO₂ in soil water. With 481 accumulating NH₄⁺ in soil, nitrification started producing NO₃⁻ and consuming O₂. N₂O didn't respond to the fertilizer 482 immediately due to enough O₂ in soil. Then when the soil became sufficiently hypoxic, N₂O fluxes entered an increasing 483 period with N₂O being produced by nitrification and denitrification processes. CO₂ fluxes were relatively low and NH₄⁺ kept

484 decreasing during this period. Finally, when soil NH_4^+ was exhausted and NO_3^- started decreasing due to denitrification, N_2O
485 fluxes then entered the decreasing period. CO_2 flux was related to urea decomposition during the leading period, and was more
486 closely related to O_2 demand in other periods. The KGML-ag predictions of N_2O and IMV captured the three periods and
487 transition points, demonstrating the connections between those variables following the description as above (Fig. 3; Fig. S5).
488 Although KGML-ag1 obtained lower IMVs prediction accuracy compared to KGML-ag2, it captured the general trends and
489 was doing better for transitions, especially in NH_4^+ predictions. KGML-ag2 overfitted on the observations and ignored the
490 correlations between IMVs, which resulted in loss in pretrain knowledge, poorer performance in the leading period, and erratic
491 predictions in the period with missing observations (before day 25).

492 **4.2 Lessons for KGML-ag development**
Interpretability of KGML-ag

493 The development of KGML-ag in our study is suitable to predict not only N_2O but also other variables, such as CO_2 , CH_4 and
494 ET, with complicated generation processes relying on the historical states. To develop a capable KGML model, we need to
495 carefully address three questions:

496
497 What kind of ML model is suitable for developing KGML? The answer could be determined by the dominant variation type
498 of the target variable in the data. If the dominant type is temporal variance, like flux variables in high temporal resolution (e.g.,
499 daily, or hourly), we should consider ML models with temporal dependency. RNN models such as GRU used in this study,
500 and CNN models such as causal CNN (Oord et al., 2016) can be good starting ML models. If the dominant type is spatial
501 variation, like variables in coarse temporal resolution (e.g., monthly or annually) but with high diversity due to soil property,
502 land cover and climate, we should consider ML models with the ability to deal with edges, hotpoints and categories, such as
503 CNN;
504

505 What physical/chemical constraints can be used to build KGML models? Although physical rules such as mass balance or
506 energy balance are conceptually straightforward and were proved capable of constraining KGML in predicting lake phosphorus
507 and temperature dynamics (Hanson et al., 2020; Read et al., 2019), they were excluded in this study according to our
508 preliminary analysis. The reason is that the mass balance equation of N in the agriculture ecosystem includes too many
509 unknown and unobservable components such as N_2 flux, NH_3 flux, N leaching, microbial N, plant N and soil/plant exchange,
510 which collectively introduce large uncertainties in balance equations and make them hard to be directly applied in the KGML-
511 ag framework. Other related physical (e.g., diffusion, solution) or chemical (e.g., nitrification, denitrification) processes cannot
512 be easily added into the KGML-ag structure as rules due to lack of understanding of the process. Instead, as mentioned in Sect.
513 2.2.4, we used hierarchical structure to enforce an architectural constraint and causal relations among variables, and pretraining
514 processes to infuse knowledge from *ecosys* to KGML-ag models.
515

Commented [14]: as a personal side comment: I think part of the difficulty is the involved many processes operate on different time scales, making the conservation constraint much harder to impose.

Commented [15R14]: This is a great point! We kind of discussed this a little bit before, on modules transition, static variables/slow change variables/fast change variables, and boundary conditions, which may be all related to your point. I will keep thinking and investigating from this point with experiments.

516 How to involve PB models in the KGML development? An advanced PB model like *ecosys* built upon biophysical and
517 biochemical rules instead of empirical relations will be a good basis to learn the process, guide the structure and provide the
518 constraints for KGML. The generated synthetic data in this study helped us get some knowledge about variables such as their
519 general trends, dynamics and correlations. Such knowledge can be transferred to KGML models from synthetic data in the
520 pretraining process, which can reduce the efforts to collect large numbers of real-world observation data. Moreover, while
521 KGML shows great potential beyond PB models, we reckon that equally important for improving N₂O modeling is to continue
522 improving our understanding of the related processes and mechanisms. Novel data collection and incorporating new
523 understanding into PB models (e.g., *ecosys*) could provide foundation to further empower KGML (see further discussion in
524 Sect. 4.3).

525

526 **4.3 Limitation and possible improvement**

527 First, the KGML-ag models in this study are limited by the available observed data. Some IMVs with high feature importance
528 scores (e.g., O₂ flux, N₂ flux) or at different depths (e.g., soil NO₃⁻ at 5 cm depth, VWC at 5 cm depth), and data out of growing
529 seasons are not included. The direct consequences are that some important processes cannot be well represented by the current
530 KGML-ag (e.g., O₂ demand and N availability for nitrification and denitrification). Further improvement of KGML should
531 consider three categories of data: target variable N₂O flux, IMVs and basic inputs (Fig. 1a). For N₂O flux observation, we lack
532 sub-hourly to sub-daily observations to capture the hot moment of emission during 0–30 days after N fertilizer applications.
533 Besides, the non-growing season can provide 35–65% of the annual direct N₂O emissions from seasonally frozen croplands
534 and lead to a 17–28 % underestimate of the global agricultural N₂O budget if ignoring its contribution (Wagner-Riddle et al.,
535 2017), but we can barely find observations from non-growing seasons. For IMVs, we found oxygen demand indicator (e.g.,
536 O₂ concentration or flux, CO₂ flux, CH₄ flux), N mass balance related variables (e.g., N₂ flux, soil NO₃⁻, soil NH₄⁺, N leaching)
537 and soil water and temperature, can be used to better constrain the processes and therefore improve the KGML performance.
538 Rohe et al. (2021) also indicated the importance of O₂, CO₂ and N₂ soil fluxes for N₂O predictions. In addition, the layerwise
539 soil observations (e.g., soil NO₃⁻, soil VWC) at 0–30 cm depth can be used to significantly improve the KGML model quality,
540 according to our feature importance analysis (Fig. S2a). Moreover, continuous monitoring on these variables during the whole
541 year is preferred rather than only during the growing season, since N₂O flux is largely influenced by previous states. To apply
542 the KGML-ag to large scale, other observational data including basic inputs of soil/crop properties (e.g., soil bulk density, pH,
543 crop type), management information (e.g., fertilizer, irrigation, tillage) and weather forcings along with N₂O flux observations
544 are critical for fine-tuning and validating the developed KGML-ag and therefore explicitly simulating the N₂O or IMVs
545 dynamics under specific conditions. Recent advances in remote sensing and machine learning have enabled estimating these
546 variables with high-resolution at a large scale (Peng et al., 2020)

547

548 Second, the physical/chemical constraints can be more comprehensive in KGML-ag models. Although current KGML-ag
549 models are well-initialized with *ecosys* synthetic data and constrained by causal relations of processes with hierarchical
550 structure, the predicted N₂O flux and IMVs can still violate some basic physical rules like mass balance. As we discussed in
551 Sec. 4.2, it will be challenging to add physical rules like mass balance equation for N in a complicated agriculture ecosystem
552 due to data limitations such as missing observations on certain key variables. Using inequalities instead of equations for mass
553 balance may be one alternative solution. For example, we could use ReLU to add in a limitation for N mass balance residues
554 which are calculated from known terms not larger than an empirical static value. Besides, better understanding of processes in
555 the N cycle from fieldworks and lab experiments can also help us design new constraints. This limitation is also partially
556 related to the data limitation and can be overcomed by involving more complete N₂O data to introduce more powerful
557 constraints to KGML-ag.

558

559 Third, the KGML-ag currently are suffering from dealing with physical/[chemical](#) boundary transitions. Boundary
560 transitions are common in the real world, such as phase change, volume solubility, and soil porosity etc. A detailed PB model
561 generally coded plenty of “if/else/switch” statements inside to deal with the boundaries. But KGML-ag models based on the
562 GRU are better at capturing continuous changes, rather than discrete changes. One solution is to include data with boundary
563 information. In this study, involving IMVs like O₂, CO₂ and N₂, which already have boundary information like water freezing
564 point, N pool volumes and other complicated boundaries related to soil/crop properties, can significantly improve the model
565 performance. The data with boundary information could be continuous observation or estimated value from existing data. By
566 using initial [values](#) to predict IMVs, KGML-ag in this study can partially solve the boundary transition problem when
567 observation data is limited. Another solution is designing new structures of KGML-ag, such as combining ReLU function or
568 including CNN model which are robust for discrete situations to the RNN models, or designing new constraints to limit the
569 model working within the thresholds.

570

571 [Finally, at the current stage we can not claim to have completely opened the black box of KGML-ag, but this framework is a](#)
572 [significant step towards this goal. For example, some ideas implemented in our study, such as using pretraining to transfer](#)
573 [knowledge from PB model to ML model, incorporating causal relations by hierarchical structure, predicting IMVs for tracking](#)
574 [middle changes and using initial values as input to reduce data demand, would shed light on the future KGML-ag framework](#)
575 [improvement.](#) Besides, we acknowledge the importance of further testing the KGML-ag over completely independent datasets,

576 but results presented in this manuscript are sufficient to justify the power of KGML as a framework. The mesocosm experiment
577 data we used in this study has provided a comprehensive set of inputs and intermediate variables in addition to the output of
578 N₂O fluxes, thus serving as a unique testbed. We expect our validation results will be more solid once more gold standard data
579 of N₂O fluxes along with other relevant inputs and intermediate variables become publicly available. Moreover, incorporating
580 more and more domain knowledge into KGML-ag will be inevitable in further improvement, but we don't think KGML-ag
581 will become inefficient as it becomes more like the PB model. In fact, to efficiently surrogate components of PB models has

582 been proposed as a research frontier in hybrid modeling for earth system science (Reichstein et al., 2019; Irrgang et al., 2021),
583 with latest advances occurring in weather forecasts (Bauer et al., 2021). By using a hybrid model, computationally inefficient
584 components of PB can be identified one by one, and be replaced with more efficient ML-based surrogates to eventually obtain
585 the most efficient model. Further KGML-ag model development will also need to balance efficiency, accuracy and
586 interpretability.

587 **5 Conclusions**

588 In this study, two KGML-ag models have been developed, validated, and tested for agricultural soil N₂O flux prediction using
589 synthetic data generated by the PB model *ecosys* and observational data from a mesocosm facility. The results show that
590 KGML-ag models can outperform PB and pure ML models in N₂O prediction in not only magnitude (KGML-ag1 $r^2 = 0.81$ vs
591 best ML model GRU $r^2 = 0.78$) but also dynamics (KGML-ag1 accuracy minus GRU accuracy, slope $\Delta^2 = 0.06$ and curvature
592 $\Delta r^2 = 0.08$). KGML-ag can also defeat the PB model *ecosys* in efficiency by completing *ecosys*'s half-hour job within a few
593 seconds. Compared to ML models, KGML-ag models can better represent complex dynamics and high peaks of N₂O flux.
594 Moreover, with IMV predictions and hierarchical structures, KGML-ag models can provide biogeophysical/chemical
595 information about key processes controlling N₂O fluxes, which will be useful for interpretable forecasting and developing
596 mitigation strategies. Data demand for the KGML-ag models is significantly reduced due to involving IMV initial values and
597 pretrain processes with synthetic data. This study demonstrated that the potential of KGML-ag application in the complex
598 agriculture ecosystem is high and illustrates possible pathways of KGML-ag development for similar tasks. Further
599 improvement of our KGML-ag models can involve general principles to further constrain the predictions through loss functions
600 or architectures, but call for more detailed, high temporal resolution N₂O observation data from field measurements.

601 **Code and Data Availability**

602 The code and data used in this study can be found at <https://doi.org/10.5281/zenodo.5504533>.

603 **Author contributions**

604 LL, ZJ, JT KG and VK conceived the study. TJG, MDE, ALF and LTM conducted mesocosm experiments and provided
605 observed data. KG, WZ and YY conducted *ecosys* simulations and provided synthetic data. LL and SX processed the data and
606 wrote the KGML-ag model code. LL, SX and SW carried the experiments out. ZJ, JT, KG, BP and WZ supervised the
607 experiments and advised on analysis from agricultural domain science perspective. VK, XJ and SX advised on the code and
608 analysis from computer science perspective. LL wrote the original draft with further editing from TK on figure and tables. SX,
609 JT, XJ, BP, YY and WZ further edited the manuscript and ZJ, KG and VK provided supervision.

610 **Competing interests**

611 The authors declare that they have no conflict of interest.

612 **References**

613 Barton, L., Wolf, B., Rowlings, D., Scheer, C., Kiese, R., Grace, P., ... & Butterbach-Bahl, K.: Sampling frequency affects
614 estimates of annual nitrous oxide fluxes, *Scientific reports*, 5(1), 1-9, 2015.

615 [Bauer, P., Dueben, P. D., Hoefer, T., Quintino, T., Schulthess, T. C., & Wedi, N. P.: The digital revolution of Earth-system
616 science. *Nature Computational Science*, 1\(2\), 104-113, 2021.](#)

617 Beucler, T., Pritchard, M., Rasp, S., Ott, J., Baldi, P., & Gentine, P.: Enforcing analytic constraints in neural networks
618 emulating physical systems, *Physical Review Letters*, 126(9), 098302, 2021.

619 Beucler, T., Rasp, S., Pritchard, M., & Gentine, P.: Achieving conservation of energy in neural network emulators for climate
620 modeling, *arXiv preprint arXiv:1906.06622*, 2019.

621 Butterbach-Bahl, K., Baggs, E. M., Dannenmann, M., Kiese, R., & Zechmeister-Boltenstern, S.: Nitrous oxide emissions from
622 soils: how well do we understand the processes and their controls? *Philosophical Transactions of the Royal Society B:
623 Biological Sciences*, 368(1621), 20130122, 2013.

624 Cho, K., Van Merriënboer, B., Bahdanau, D., & Bengio, Y.: On the properties of neural machine translation: Encoder-decoder
625 approaches, *arXiv preprint arXiv:1409.1259*, 2014.

626 Chung, Junyoung, Caglar Gulcehre, KyungHyun Cho, and Yoshua Bengio.: Empirical evaluation of gated recurrent neural
627 networks on sequence modeling, *arXiv preprint arXiv:1412.3555*, 2014.

628 Daw, A., Thomas, R. Q., Carey, C. C., Read, J. S., Appling, A. P., & Karpatne, A.: Physics-guided architecture (pga) of neural
629 networks for quantifying uncertainty in lake temperature modeling, In *Proceedings of the 2020 siam international conference
630 on data mining* (pp. 532-540), Society for Industrial and Applied Mathematics, 2020.

631 Del Grosso, S. J., Parton, W. J., Mosier, A. R., Ojima, D. S., Kulmala, A. E., & Phongpan, S.: General model for N₂O and N₂
632 gas emissions from soils due to denitrification, *Global biogeochemical cycles*, 14(4), 1045-1060, 2020.

633 Fassbinder, J. J., Schultz, N. M., Baker, J. M., & Griffis, T. J.: Automated, Low-Power Chamber System for Measuring Nitrous
634 Oxide Emissions, *Journal of environmental quality*, 42, 606. doi: 10.2134/jeq2012.0283, 2013.

635 Fassbinder, J. J., Griffis, T. J., & Baker, J. M.: Evaluation of carbon isotope flux partitioning theory under simplified and
636 controlled environmental conditions, *Agricultural and forest meteorology*, 153, 154-164, 2012.

637 Forster, P., Storelvmo, T., Armour, K. , Collins, W., ... & Zhang, H.: The Earth's Energy Budget, Climate Feedbacks, and
638 Climate Sensitivity. In: *Climate Change 2021: The Physical Science Basis. Contribution of Working Group I to the Sixth
639 Assessment Report of the Intergovernmental Panel on Climate Change*, Cambridge University Press. In Press, 2021.

640 Gilhespy, S. L., Anthony, S., Cardenas, L., Chadwick, D., del Prado, A., Li, C., ... & Yeluripati, J. B.: First 20 years of DNDC
641 (DeNitrification DeComposition): model evolution, *Ecological modelling*, 292, 51-62, 2014.

642 Grant, R. F.: Modeling Carbon and Nitrogen Dynamics for Soil Management, (Boca Raton, FL: CRC Press) A review of the
643 Canadian ecosystem model ecosys 173–264, 2021.

644 Grant, R. F., & Pattey, E.: Modelling variability in N₂O emissions from fertilized agricultural fields, *Soil Biology and*
645 *Biochemistry*, 35(2), 225-243, 2003.

646 [Grant, R. F., & Pattey, E.: Temperature sensitivity of N₂O emissions from fertilized agricultural soils: Mathematical modeling](#)
647 [in ecosys. *Global biogeochemical cycles*, 22\(4\), 2008.](#)

648 [Grant, R. F., Neftel, A., & Calanca, P.: Ecological controls on N₂O emission in surface litter and near-surface soil of a managed](#)
649 [grassland: modelling and measurements, *Biogeosciences*, 13\(12\), 3549-3571, 2016.](#)

650 Grant, R. F., Neftel, A., & Calanca, P.: Ecological controls on N₂O emission in surface litter and near-surface soil of a managed
651 grassland: modelling and measurements, *Biogeosciences*, 13(12), 3549-3571, 2016.

652 Grant, R. F., Pattey, E., Goddard, T. W., Kryzanowski, L. M., & Puurveen, H.: Modeling the effects of fertilizer application
653 rate on nitrous oxide emissions, *Soil Science Society of America Journal*, 70(1), 235-248, 2006.

654 Hamrani, A., Akbarzadeh, A., & Madramootoo, C. A.: Machine learning for predicting greenhouse gas emissions from
655 agricultural soils, *Science of The Total Environment*, 741, 140338, 2020.

656 Hanson, P. C., Stillman, A. B., Jia, X., Karpatne, A., Dugan, H. A., Carey, C. C., ... & Kumar, V.: Predicting lake surface
657 water phosphorus dynamics using process-guided machine learning, *Ecological Modelling*, 430, 109136, 2020.

658 Holzworth, D. P., Huth, N. I., deVoil, P. G., Zurcher, E. J., Herrmann, N. I., McLean, G., ... & Keating, B. A.: APSIM—
659 evolution towards a new generation of agricultural systems simulation, *Environmental Modelling & Software*, 62, 327-350,
660 2014.

661 [Irrgang, C., Boers, N., Sonnewald, M., Barnes, E. A., Kadow, C., Staneva, J., & Saynisch-Wagner, J.: Towards neural Earth](#)
662 [system modelling by integrating artificial intelligence in Earth system science. *Nature Machine Intelligence*, 3\(8\), 667-674,](#)
663 [2021.](#)

664 Jia, X., Willard, J., Karpatne, A., Read, J. S., Zwart, J. A., Steinbach, M., & Kumar, V.: Physics-guided machine learning for
665 scientific discovery: An application in simulating lake temperature profiles, *ACM/IMS Transactions on Data Science*, 2(3), 1-
666 26, 2021.

667 Jia, X., Willard, J., Karpatne, A., Read, J., Zwart, J., Steinbach, M., & Kumar, V.: Physics guided RNNs for modeling
668 dynamical systems: A case study in simulating lake temperature profiles, In *Proceedings of the 2019 SIAM International*
669 *Conference on Data Mining* (pp. 558-566), Society for Industrial and Applied Mathematics, 2019.

670 Karpatne, A., Atluri, G., Faghmous, J. H., Steinbach, M., Banerjee, A., Ganguly, A., ... & Kumar, V.: Theory-guided data
671 science: A new paradigm for scientific discovery from data, *IEEE Transactions on knowledge and data engineering*, 29(10),
672 2318-2331, 2017.

673 Keating, B. A., Carberry, P. S., Hammer, G. L., Probert, M. E., Robertson, M. J., Holzworth, D., ... & Smith, C. J.: An overview
674 of APSIM, a model designed for farming systems simulation, *European journal of agronomy*, 18(3-4), 267-288, 2003.

675 Khandelwal, A., Xu, S., Li, X., Jia, X., Stienbach, M., Duffy, C., ... & Kumar, V.: Physics guided machine learning methods
676 for hydrology, arXiv preprint arXiv:2012.02854, 2020.

677 Kim, T., Jin, Z., Smith, T., Liu, L., Yang, Y., Yang, Y., ... & Zhou, W.: Quantifying nitrogen loss hotspots and mitigation
678 potential for individual fields in the US Corn Belt with a metamodeling approach, Environmental Research Letters, 2021.

679 Kraft, B., Jung, M., Körner, M., Koirala, S., & Reichstein, M.: Towards hybrid modeling of the global hydrological cycle,
680 Hydrology and Earth System Sciences Discussions, 1-40, 2021.

681 Meyer, D., Nagler, T., & Hogan, R. J.: Copula-based synthetic data augmentation for machine-learning emulators.
682 Geoscientific Model Development, 14(8), 5205-5215, 2021.

683 Miller, L. T. , Griffis, T. J., Erickson, M. D., Turner, P. A., Deventer, M. J., Chen, Z., Yu, Z., Venterea, R.T., Baker, J. M.,
684 and Frie, A. L.: Response of nitrous oxide emissions to future changes in precipitation and individual rain events, Journal of
685 Environmental Quality, In review, 2021

686 Miller, L. T., Assessing Agricultural Nitrous Oxide Emissions and Hot Moments Using Mesocosm Simulations, (Master
687 Thesis, University of Minnesota) Retrieved from the University of Minnesota Digital Conservancy,
688 <https://hdl.handle.net/11299/219276>, 2021

689 Nećpálová, M., Anex, R. P., Fienan, M. N., Del Grosso, S. J., Castellano, M. J., Sawyer, J. E., ... & Barker, D. W.:
690 Understanding the DayCent model: Calibration, sensitivity, and identifiability through inverse modeling, Environmental
691 Modelling & Software, 66, 110-130, 2015.

692 Oord, A. V. D., Dieleman, S., Zen, H., Simonyan, K., Vinyals, O., Graves, A., ... & Kavukcuoglu, K.: Wavenet: A generative
693 model for raw audio, arXiv preprint arXiv:1609.03499, 2016.

694 Pachauri, R. K., Allen, M. R., Barros, V. R., Broome, J., Cramer, W., Christ, R., ... & van Ypserle, J. P.: Climate change 2014:
695 synthesis report. Contribution of Working Groups I, II and III to the fifth assessment report of the Intergovernmental Panel on
696 Climate Change (p. 151). Ipcc, 2014.

697 Read, J. S., Jia, X., Willard, J., Appling, A. P., Zwart, J. A., Oliver, S. K., ... & Kumar, V.: Process-guided deep learning
698 predictions of lake water temperature, Water Resources Research, 55(11), 9173-9190, 2019.

699 Peng, B., Guan, K., Tang, J., Ainsworth, E. A., Asseng, S., Bernacchi, C. J., ... & Zhou, W.: Towards a multiscale crop
700 modelling framework for climate change adaptation assessment, Nature plants, 6(4), 338-348, 2020.

701 [Reichstein, M., Camps-Valls, G., Stevens, B., Jung, M., Denzler, J., & Carvalhais, N.: Deep learning and process understanding
702 for data-driven Earth system science. Nature, 566\(7743\), 195-204, 2019.](#)

703 Robertson, M., BenDor, T. K., Lave, R., Riggsbee, A., Ruhl, J. B., & Doyle, M.: Stacking ecosystem services, Frontiers in
704 Ecology and the Environment, 12(3), 186-193, 2014.

705 Rohe, L., Apelt, B., Vogel, H. J., Well, R., Wu, G. M., & Schlüter, S.: Denitrification in soil as a function of oxygen availability
706 at the microscale, Biogeosciences, 18(3), 1185-1201, 2021.

707 Saha, D., Basso, B., & Robertson, G. P.: Machine learning improves predictions of agricultural nitrous oxide (N_2O) emissions
708 from intensively managed cropping systems, Environmental Research Letters, 16(2), 024004, 2021.

709 Solazzo, E., Crippa, M., Guizzardi, D., Muntean, M., Choulga, M., & Janssens-Maenhout, G.: Uncertainties in the Emissions
710 Database for Global Atmospheric Research (EDGAR) emission inventory of greenhouse gases, *Atmospheric Chemistry and*
711 *Physics*, 21(7), 5655-5683, 2021.

712 Solazzo, E., Crippa, M., Guizzardi, D., Muntean, M., Choulga, M., & Janssens-Maenhout, G.: Uncertainties in the Emissions
713 Database for Global Atmospheric Research (EDGAR) emission inventory of greenhouse gases, *Atmospheric Chemistry and*
714 *Physics*, 21(7), 5655-5683, 2021.

715 Syakila, A., & Kroeze, C.: The global nitrous oxide budget revisited, *Greenhouse gas measurement and management*, 1(1),
716 17-26, 2011.

717 Thompson, R. L., Lassaletta, L., Patra, P. K., Wilson, C., Wells, K. C., Gressent, A., ... & Canadell, J. G.: Acceleration of
718 global N₂O emissions seen from two decades of atmospheric inversion, *Nature Climate Change*, 9(12), 993-998, 2019.

719 Thornley, J. H., & France, J.: Mathematical models in agriculture: quantitative methods for the plant, animal and ecological
720 sciences, Cabi, 2007.

721 Tian, H., Xu, R., Canadell, J. G., Thompson, R. L., Winiwarter, W., Suntharalingam, P., ... & Yao, Y.: A comprehensive
722 quantification of global nitrous oxide sources and sinks, *Nature*, 586(7828), 248-256, 2020.

723 [Venterea, R. T., Mahajan, B., & Dolan, M. S.: Fertilizer source and tillage effects on yield-scaled nitrous oxide emissions in](#)
724 [a corn cropping system. *Journal of Environmental Quality*, 40\(5\), 1521-1531, 2011.](#)

725 Wagner-Riddle, C., Congreves, K. A., Abalos, D., Berg, A. A., Brown, S. E., Ambadan, J. T., ... & Tenuta, M.: Globally
726 important nitrous oxide emissions from croplands induced by freeze-thaw cycles, *Nature Geoscience*, 10(4), 279-283, 2017.

727 Willard, J., Jia, X., Xu, S., Steinbach, M., & Kumar, V.: Integrating Scientific Knowledge with Machine Learning for
728 Engineering and Environmental Systems, *arXiv preprint arXiv:2003.04919*, 2020.

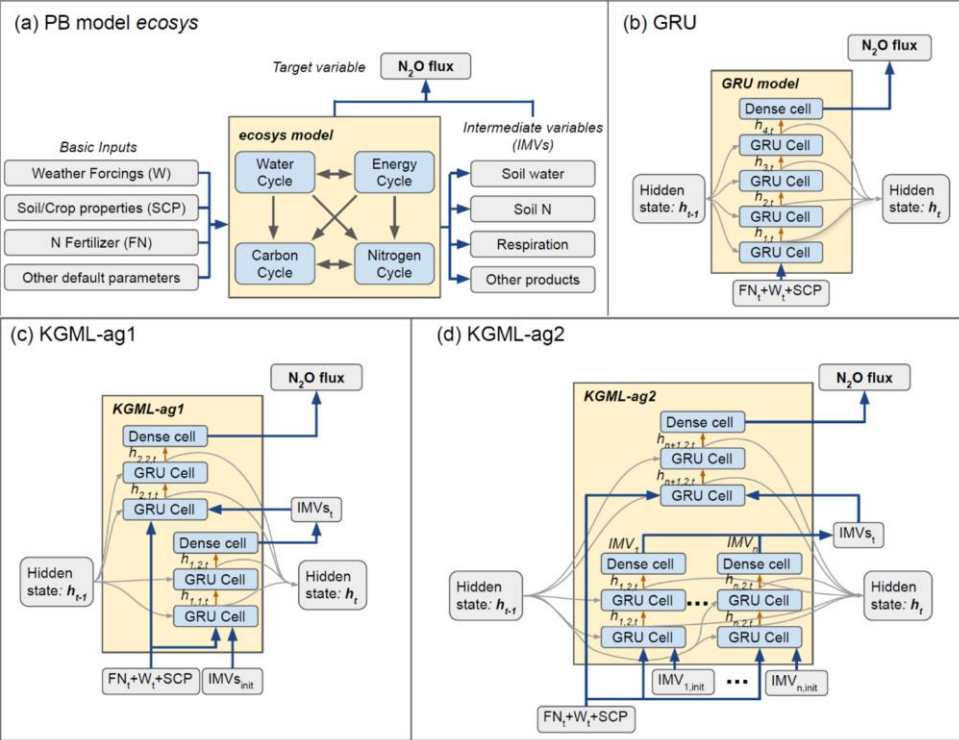
729 [Yang, Y., Liu, L., Zhou, W., Guan, K., Kim, T., Tang, J., Peng, B., Zhu, P., Grant, R. F., Griffis, T. J., Jin, Z.: Distinct driving](#)
730 [mechanisms of non-growing season N₂O emissions call for spatial-specific mitigation strategies in the US Midwest. *One Earth*.](#)
731 [Submitted, 2022.](#)

732 Zhang, Y., & Niu, H.: The development of the DNDC plant growth sub-model and the application of DNDC in agriculture: a
733 review, *Agriculture, Ecosystems & Environment*, 230, 271-282, 2016.

734 Zhang, Y., Li, C., Zhou, X., & Moore III, B.: A simulation model linking crop growth and soil biogeochemistry for sustainable
735 agriculture, *Ecological modelling*, 151(1), 75-108, 2002.

736

737



738
739 Figure 1: The model [structures](#). a) The ecosys model [frame](#); b) Gated recurrent unit (GRU) model [frame](#); c) KGML-ag1
740 model [with a frame of hierarchical structure](#); d) KGML-ag2 model [with a frame of hierarchical structure with separated GRU](#)
741 modules for IMV predictions. Specifically, in our KGML model design, weather forcings (W) include temperature (TMAX, TDIF),
742 precipitation (PRECN), radiation (RADN), humidity (HMAX and HDIF) and wind speed (WIND); soil/crop properties (SCP)
743 include bulk density (TBKDS), sand content (TCSAND), silt content (TCSILT), pH (TPH), cation exchange capacity (TCEC), soil
744 organic carbon (TSOC), planting day of the year (PDOY) and crop type (CROPT); IMVs include CO₂ flux, soil NO₃⁻ concentration,
745 soil NH₄⁺ concentration, and soil volumetric water content (VWC).

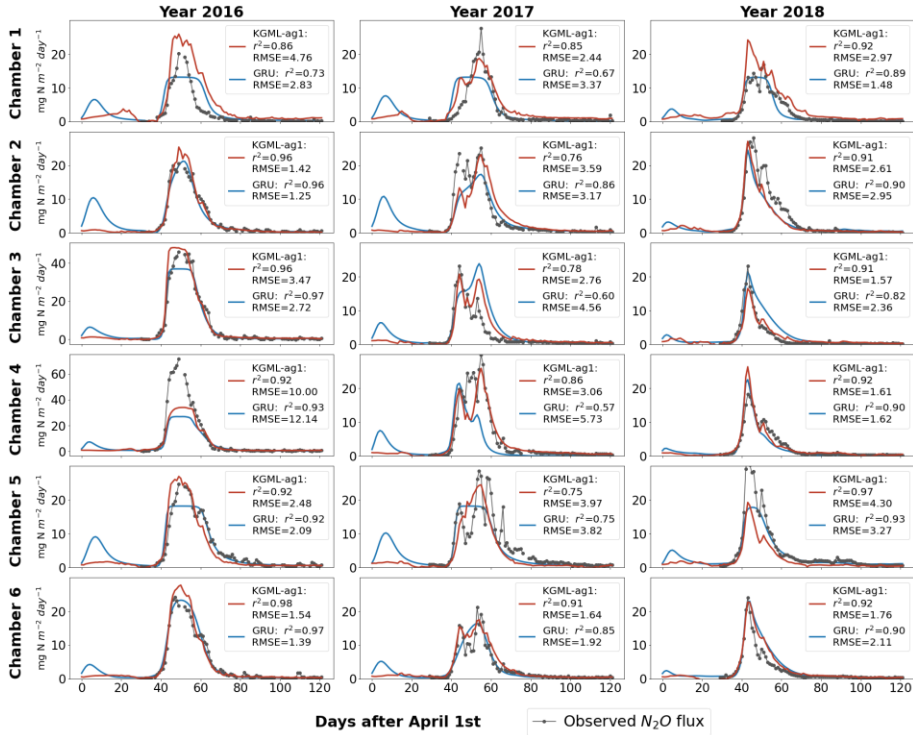
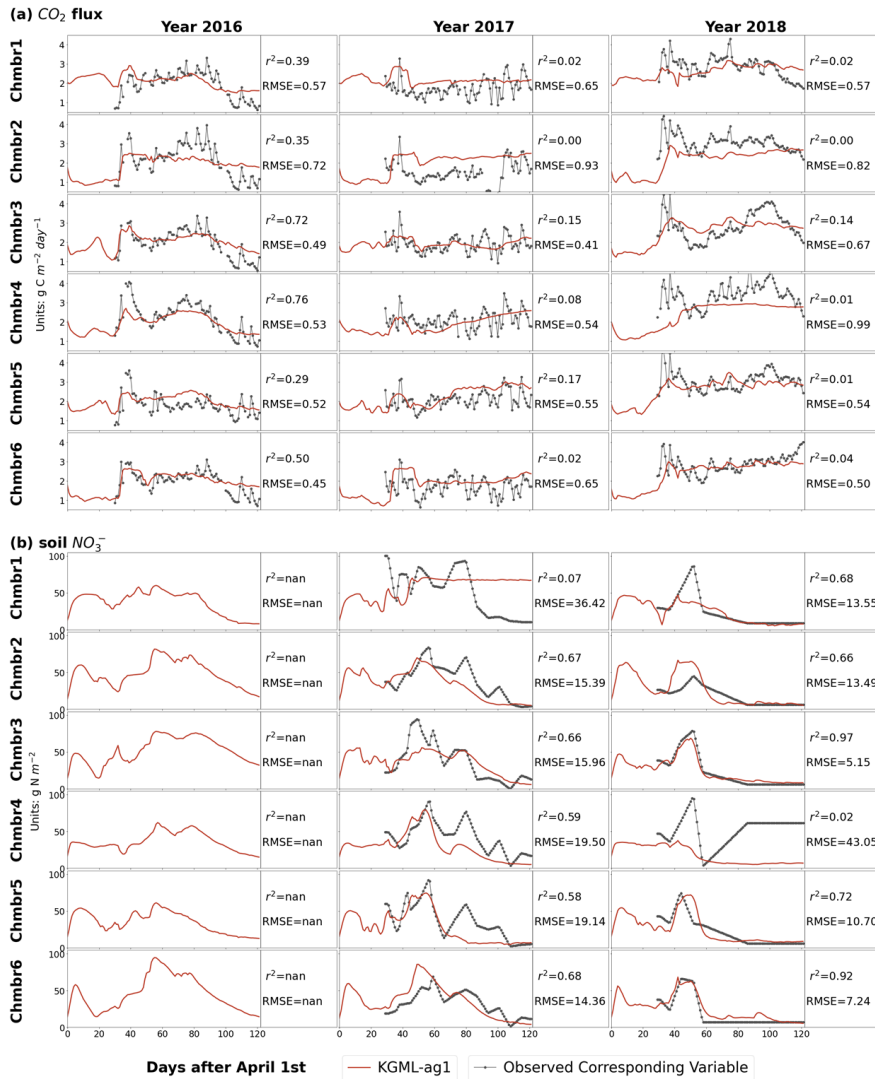
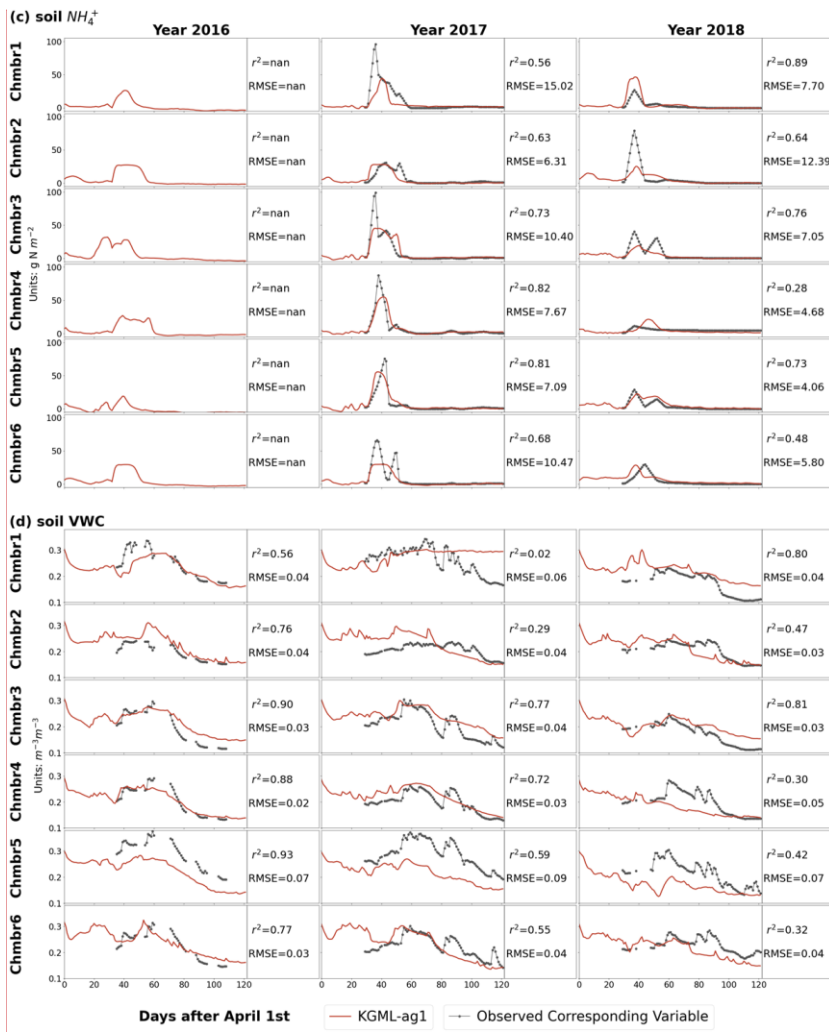


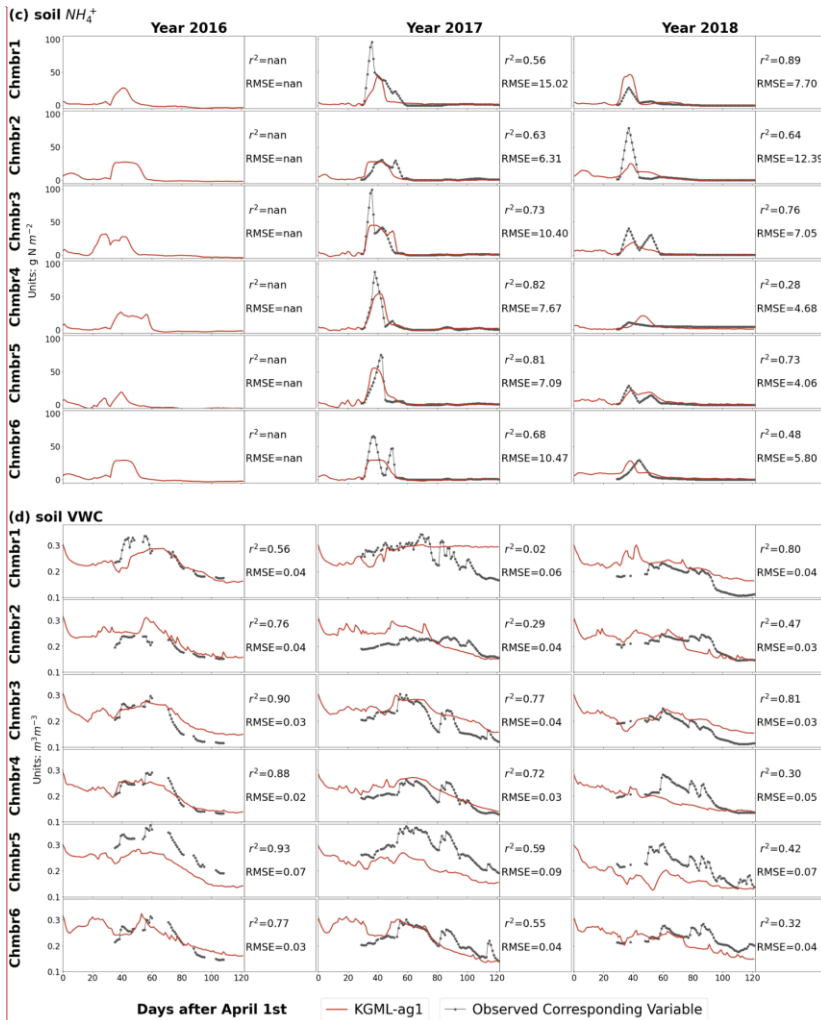
Figure 2: N₂O flux time series comparisons among pure non-pretrained GRU predictions (blue line), KGML-ag1 predictions (red line) and observations (black line-dot) from cross-validation. The N₂O flux unit is mg N m⁻² day⁻¹.



752
753
754
Figure 3: IMVs prediction from KGML-ag1. The black-dot line represents observations and the red line represents the results from
KGML-ag1. Chmb is the abbreviation for chamber. r^2 and RMSE are calculated and present in each year and chamber. The CO₂
flux and soil NO₃ concentration units are g C m⁻² day⁻¹ and g N m⁻², respectively.

755





Commented [16]: A typo of VWC units has been fixed.

757

758
759
760

Figure 3 Contd.: IMVs prediction from KGML-ag1. The black-dot line represents observations and the red line represents the results from KGML-ag1. Chmb is the abbreviation for chamber. r^2 and RMSE are calculated and present in each year and chamber. The soil NH_4^+ concentration and soil VWC units are g N m^{-2} and $\text{m}^3 \text{m}^{-3}$, respectively.

761

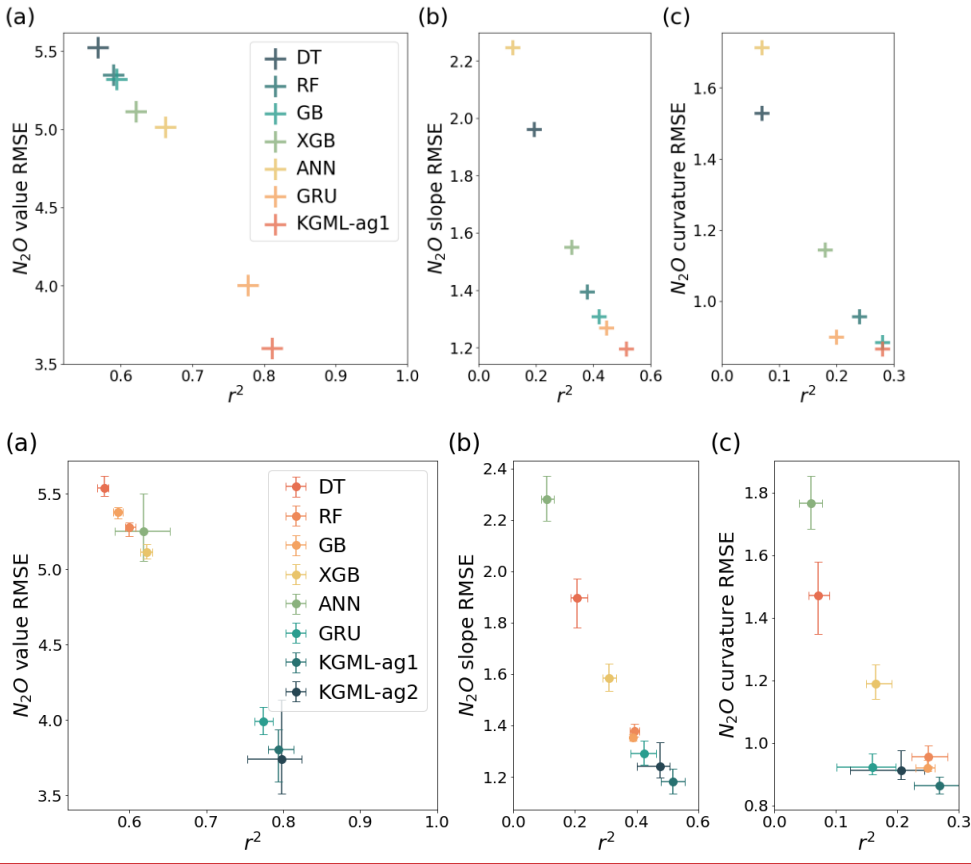
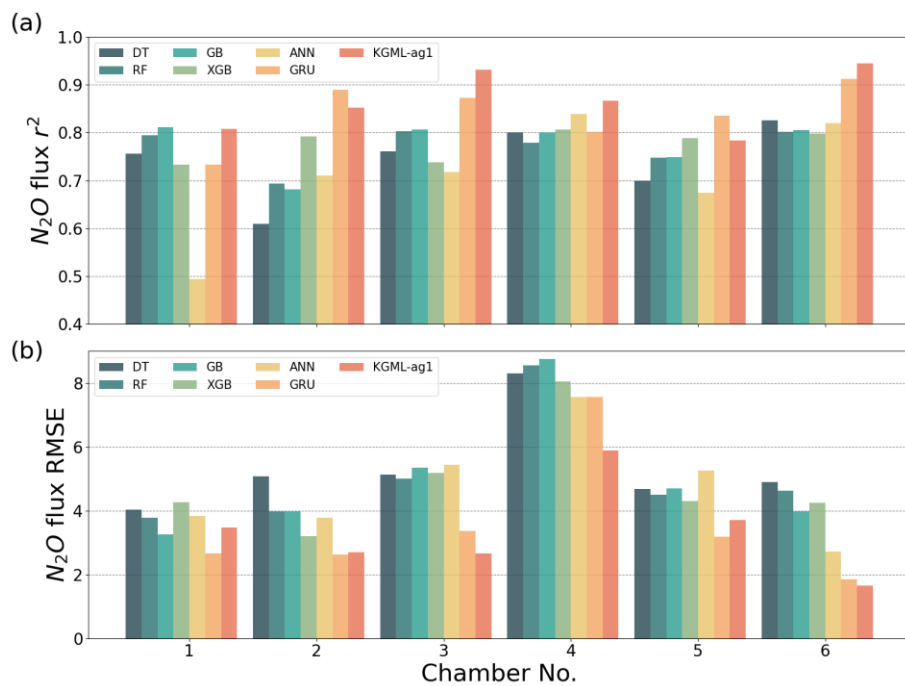
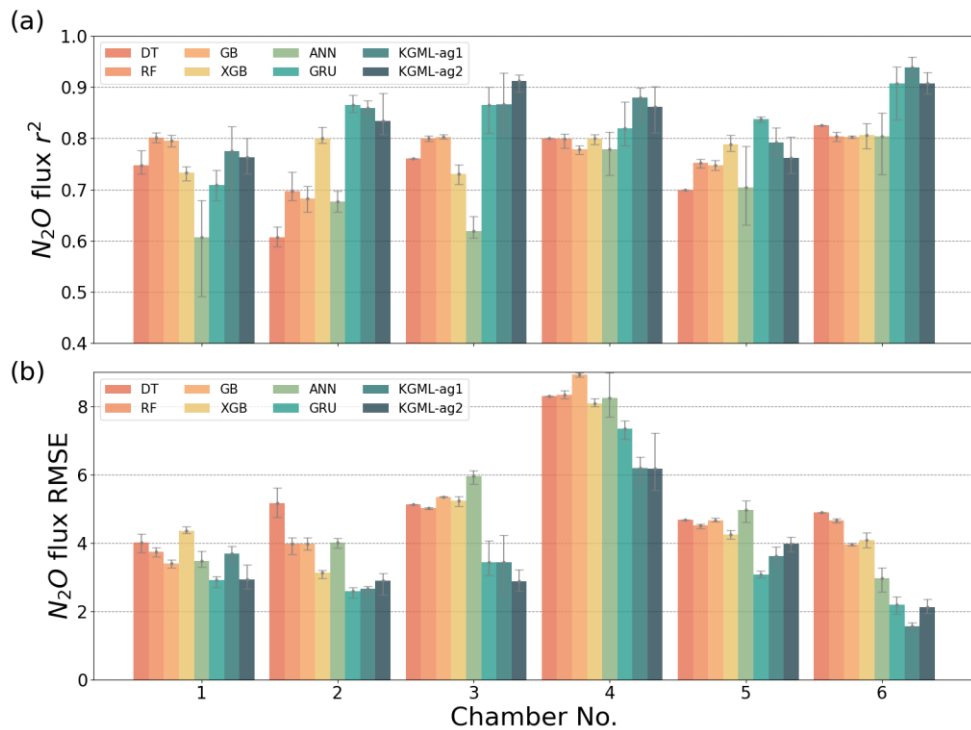


Figure 4: The comparisons of overall prediction accuracy for N_2O value (a), 1st order gradient (slope, b) and 2nd order gradient (curvature, c) between four tree-based ML models (DT, RF, GB and XGB), two deep learning models (ANN and GRU) and KGML-ag4 models. Different color symbols represent the different models. The x- and y-error bars are coming from the maximum and minimum scores of ensemble experiments. The dot represents the mean score of the ensemble experiments.





Formatted: Font: (Default) Arial, (Asian) Arial, 11 pt

769
 770 Figure 5: The comparisons of N_2O flux prediction accuracy r^2 (a) and (b) RMSE, between four tree-based ML models (DT, RF, GB
 771 and XGB), two deep learning models (ANN and GRU) and KGML-ag1 models in 6 chambers. The gray error bars are coming from
 772 the maximum and minimum scores of ensemble experiments.

Table 1: Pretrain results for different model and IMV combinations using *ecosys* synthetic data.

No.	Pretrain Model	Input Feature N	N ₂ O		CO ₂		NO ₃ ⁻		NH ₄ ⁺		VWC	
			r ²	RMSE	r ²	NRMSE	r ²	NRMSE	r ²	NRMSE	r ²	NRMSE
1	GRU+76IMVs	76 IMVs+FN+7Ws+8SCP	0.98	0.54	-- ^a	--	--	--	--	--	--	--
2	GRU+IMVcb1	4 IMVs+FN+7Ws+8SCP	0.92	1.15	--	--	--	--	--	--	--	--
3	GRU+IMVcb2	3 IMVs+FN+7Ws+8SCP	0.90	1.26	--	--	--	--	--	--	--	--
4	GRU	FN+7Ws+8SCP	0.89	1.37	--	--	--	--	--	--	--	--
5	KGML-ag1+IMVcb1_ini	FN+7Ws+8SCP+4IMV_ini	0.90	1.24	0.91	0.06	0.95	0.03	0.98	0.03	0.95	0.04
6	KGML-ag1+IMVcb2_ini	FN+7Ws+8SCP+3IMV_ini	0.90	1.26	--	--	0.94	0.03	0.97	0.03	0.95	0.04
7	KGML-ag2+IMVcb1_ini	FN+7Ws+8SCP+4IMV_ini	0.90	1.27	0.92	0.05	0.95	0.02	0.98	0.03	0.96	0.04
8	KGML-ag2+IMVcb2_ini	FN+7Ws+8SCP+3IMV_ini	0.91	1.19	--	--	0.95	0.00	0.99	0.02	0.95	0.04

^aThe empty slot indicates that the model does not predict that variable.

Table 2: Prediction accuracy comparisons between non-pretrained GRU model and KGML-ag1. Pretrain results for different model and IMV combinations using *ecosys* synthetic data.

N ₂ O, KGML-ag1 minus GRU			N ₂ O 1st order gradient, KGML-ag1 minus GRU				N ₂ O 2nd order gradient, KGML-ag1 minus GRU						
	No.	All time ^b	Day 30-80	Day 40-65	Day 45-60	All time	Day 30-80	Day 40-65	Day 45-60	All time	Day 80	30-Day 65	40-Day 45-60
Δr^2 ^a	All data	0.03 ^c	0.04	0.07	0.10	0.07	0.07	0.07	0.15	0.08	0.08	0.09	0.11
	Chamber1	0.07	0.10	0.20	0.13	0.18	0.18	0.19	0.14	0.08	0.09	0.09	0.02
	Chamber2	-0.04	-0.05	-0.07	-0.05	0.08	0.09	0.09	0.16	0.20	0.20	0.20	0.23
	Chamber3	0.06	0.06	0.08	0.06	0.04	0.04	0.04	0.13	-0.01	-0.01	-0.01	0.07
	Chamber4	0.06	0.08	0.12	0.07	0.05	0.05	0.05	0.14	0.07	0.07	0.08	0.12
	Chamber5	-0.05	-0.06	-0.07	-0.03	0.09	0.09	0.10	0.16	0.13	0.13	0.15	0.11
	Chamber6	0.03	0.04	0.08	0.17	0.14	0.14	0.15	0.22	0.12	0.13	0.14	0.23
ARMSE ^a	All data	-0.41	-0.56	-0.84	-1.19	-0.07	-0.10	-0.14	-0.20	-0.03	-0.05	-0.07	-0.08
	Chamber1	0.80	1.06	1.21	1.70	0.00	0.00	-0.02	0.00	0.05	0.07	0.10	0.18
	Chamber2	0.08	0.11	0.07	-0.04	-0.10	-0.13	-0.18	-0.14	-0.10	-0.14	-0.19	-0.22
	Chamber3	-0.71	-0.96	-1.30	-2.09	0.03	0.04	0.07	-0.25	0.09	0.13	0.17	0.08
	Chamber4	-1.68	-2.27	-3.09	-3.81	-0.11	-0.15	-0.21	-0.26	-0.05	-0.07	-0.09	-0.16
	Chamber5	0.53	0.69	0.86	0.99	-0.10	-0.14	-0.20	-0.23	-0.09	-0.12	-0.18	-0.14
	Chamber6	-0.20	-0.27	-0.37	-0.61	-0.14	-0.20	-0.29	-0.33	-0.07	-0.10	-0.15	-0.19

^aThe difference of r² (Δr^2), and difference of RMSE (Δ RMSE, units are mg N m⁻² day⁻¹, mg N m⁻² day⁻², mg N m⁻² day⁻³ for N₂O value, 1st order gradient and 2nd order gradient, respectively) were calculated by values from KGML-ag1 minus values from GRU.

^bResults from different time windows of different chambers during the period of April 1st-July31st (Days1-122) were detected.

^cBlue cells mean KGML-ag1 outperforms GRU, while yellow cells mean the opposite.

784

785

786

Table 3: Experiments for measuring GRU and KGML-ag models performance, and influence of pretraining process, training data augmentation and IMV initial values.

No.	Retrain	Model	Experiment	N ₂ O 1st order gradient				N ₂ O 2nd order gradient				CO ₂			NO ₃ ⁻			NH ₄ ⁺			VWC	
				r ²	RMSE	r ²	RMSE	r ²	RMSE	r ²	NRMSE	r ²	NRMSE	r ²	NRMSE	r ²	NRMSE	r ²	NRMSE	r ²	NRMSE	
1	GRU	GRU, baseline ^a	No Pretrain	0.78	4.00	0.45	1.27	0.20	0.90	-- ^b	--	--	--	--	--	--	--	--	--	--	--	
2	GRU		Pretrain	0.80	3.77	0.57	1.12	0.34	0.82	--	--	--	--	--	--	--	--	--	--	--	--	
3	KGML-ag1+	Original	IMVcb1_ini	0.81	3.60	0.51	1.20	0.28	0.87	0.37	0.14	0.39	0.21	0.60	0.09	0.33	0.18					
4	KGML-ag1+	Original	IMVcb2_ini	0.80	3.71	0.49	1.22	0.21	0.91	--	--	0.37	0.22	0.53	0.10	0.33	0.19					
5	KGML-ag2+	Original	IMVcb1_ini	0.79	3.77	0.48	1.23	0.22	0.90	0.74	0.09	0.46	0.18	0.66	0.08	0.84	0.08					
6	KGML-ag2+	Original	IMVcb2_ini	0.78	3.91	0.47	1.24	0.20	0.91	--	--	0.49	0.18	0.69	0.08	0.84	0.08					
7	KGML-ag1+	No	IMVcb1_ini	0.80	3.73	0.49	1.22	0.22	0.90	0.38	0.14	0.38	0.21	0.61	0.09	0.37	0.17					
8	KGML-ag1+	No	IMVcb2_ini	0.77	4.04	0.41	1.31	0.13	0.95	--	--	0.38	0.21	0.53	0.10	0.35	0.18					
9	KGML-ag2+	No	IMVcb1_ini	0.76	4.06	0.45	1.27	0.16	0.95	0.69	0.10	0.21	0.25	0.60	0.09	0.80	0.09					
10	KGML-ag2+	No	IMVcb2_ini	0.74	4.27	0.48	1.23	0.21	0.90	--	--	0.40	0.21	0.60	0.09	0.81	0.09					
11	KGML-ag1+	Zero initial	IMVcb1_ini	0.48	6.27	0.26	1.49	0.08	1.00	0.19	0.16	0.25	0.25	0.47	0.12	0.14	0.25					
12	KGML-ag1+	Zero initial	IMVcb2_ini	0.49	5.94	0.31	1.41	0.13	0.95	--	--	0.31	0.25	0.38	0.13	0.24	0.25					
13	KGML-ag2+	Zero initial	IMVcb1_ini	0.48	6.05	0.12	1.66	0.01	1.09	0.58	0.12	0.34	0.25	0.21	0.13	0.56	0.31					
14	KGML-ag2+	Zero initial	IMVcb2_ini	0.39	6.60	0.15	1.59	0.04	1.01	--	--	0.16	0.27	0.27	0.12	0.53	0.31					

^aGray region includes the experiments with original simulation settings as described in Sec. 2 and dark gray refers to the baseline GRU simulation; Blue region includes the experiments without data augmentation during the finetuning process; And yellow region includes the experiments of replacing original IMV initial values with zeros.

^bThe empty slot indicates that the model does not predict that variable.

791